JACS
JOURNAL OF THE AMERICAN CHEMICAL SOCIETY

Article

Dual Role of Doubly Reduced Arylboranes as Dihydrogen- and Hydride-Transfer Catalysts

Esther von Grotthuss, Sven E. Prey, Michael Bolte, Hans-Wolfram Lerner, and Matthias Wagner

J. Am. Chem. Soc., **Just Accepted Manuscript** • DOI: 10.1021/jacs.9b01998 • Publication Date (Web): 15 Mar 2019

Just Accepted

ACS Publications

is published by the American Chemical Society. 1155 Sixteenth Street N.W., Washington, DC 20036

Dual Role of Doubly Reduced Arylboranes as Dihydrogen- and Hydride-Transfer Catalysts

Esther von Grotthuss, Sven E. Prey, Michael Bolte, Hans-Wolfram Lerner, and Matthias Wagner*

Institut für Anorganische und Analytische Chemie, Goethe-Universität Frankfurt, Max-von-Laue-Straße 7, D-60438 Frankfurt am Main, Germany

ABSTRACT: Doubly reduced 9,10-dihydro-9,10-diboraanthracenes (DBAs) are introduced as catalysts for hydrogenation as well as hydride-transfer reactions. The required alkali metal salts M_2[DBA] are readily accessible from the respective neutral DBAs and Li metal, Na metal, or KC_8. In the first step, the ambiphilic M_2[DBA] activate H_2 in a concerted, metal-like fashion. The rates of H_2 activation strongly depend on the B-bonded substituents and the counter cations. Smaller substituents (*e.g.*, H, Me) are superior to bulkier groups (*e.g.*, Et, *p*Tol), and a Mes substituent is even prohibitively large. Li^+ ions, which form persistent contact ion pairs with $[DBA]^{2-}$, slow down the H_2-addition rate to a higher extent than more weakly coordinating Na^+/K^+ ions. For the hydrogenation of unsaturated compounds, we identified Li_2[**4**] (Me substituents at boron) as the best performing catalyst; its substrate scope encompasses Ph(H)C=N*t*Bu, $Ph_2C=CH_2$, and anthracene. The conversion of E–Cl to E–H bonds (E = C, Si, Ge, P) was best achieved by using Na_2[**4**]. The latter protocol provides facile access also to $Me_2Si(H)Cl$, a most important silicone building block. Whereas the H_2-transfer reaction regenerates the dianion $[\mathbf{4}]^{2-}$ and is thus immediately catalytic, the H^--transfer process releases the neutral **4**, which has to be recharged by Na metal before it can enter the cycle again. In order to avoid Wurtz-type coupling of the substrate, the reduction of **4** must be performed in the absence of the element halide, which demands an alternating process management (similar to the industrial anthraquinone process).

INTRODUCTION

In addition to transition metal complexes and Frustrated Lewis Pairs (FLPs),[1] main group species in low oxidation states are emerging as a third class of compounds capable of H_2 activation.[2] Three subclasses can be distinguished: *1. Single-site activators* possess a coordinatively unsaturated atom bearing a lone pair of electrons together with an orthogonally positioned vacant orbital. Examples include borylenes, carbenes, and silylenes (cf. Bertrand's borylene[3] in Scheme 1). In all these cases the result is an oxidative addition of H_2, but the actual reaction mechanisms differ between electrophilic (B, Si) and nucleophilic (C) activation.[4] *2. Compounds containing two mutually connected active sites* are known with single as well as multiple bonds (cf. Yamashita's diborane(4)[5] in Scheme 1). As a general motif, the initial reaction step involves donation of charge from the σ orbital of H_2 to only one of the active sites. In a synergic electron flow, σ- or π-electron density from between the main group centers accepts a proton and thereby splits the H_2 molecule.[6] *3. Compounds containing two spatially separated active sites* can nevertheless achieve a cooperative action of the latter on the H_2 substrate.[7] For the dianion salt Li_2[**1**] (Scheme 1),[8] quantum-chemical calculations revealed that the HOMO and the LUMO of $[\mathbf{1}]^{2-}$ have the same local symmetries as the σ* and σ orbitals, respectively, of the H–H bond. The spatial disposition of the frontier orbitals of $[\mathbf{1}]^{2-}$ is also ideally suited for interaction with H_2, which suggests a concerted, homolytic addition across both boron atoms.

The discovery of main group compounds rivaling transition metal complexes for the cleavage of the thermodynamically stable H–H bond represented a paradigm shift in fundamental research.[9] In terms of synthetic applications, however, the H_2-addition products should not be inert thermodynamic sinks, but rather have the potential to hand over the received hydrogen atoms to an added substrate molecule. For FLPs such reactivity has been amply demonstrated and led to the devel-

Scheme 1. Examples of H_2 Activation with Boron Species in Low Oxidation States: Single-Site Activator (top), Compound Containing Two Mutually Connected Active Sites (middle), and Compound Containing Two Spatially Separated Active Sites (bottom). Dip = 2,6-diisopropylphenyl; Cy = spiro-cyclohexyl.

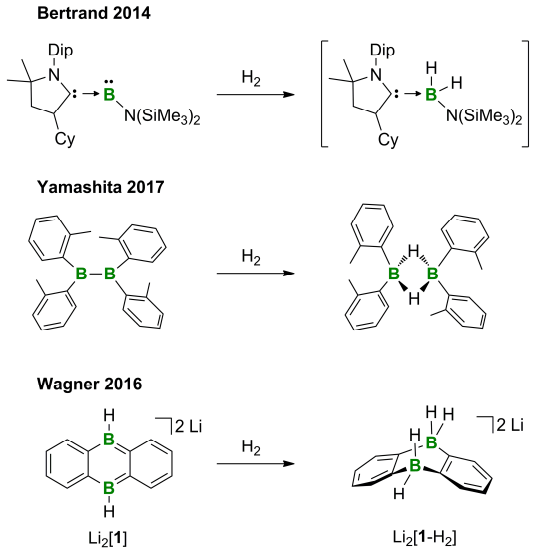

opment of entire catalytic cycles.[10] In contrast, hydrogenation reactions mediated by main group species in low oxidation states are essentially unknown[11] and even reversible H_2 activation has rarely been reported. One of the few examples is the singlet biradicaloid $[P(\mu NTer)]_2$ (Ter = 2,6-bis(mesityl)-phenyl), which adds H_2 at room temperature across its phosphorus atoms and releases it again at 60 °C.[12] Our group recently observed a dynamic addition/elimination equilibrium between H_2 and a derivative of Li_2[**1**] bearing two alkynyl instead of hydrogen substituents at its boron atoms (cf. Li_2[**2**] in Scheme 2).[8]

Herein we use the parent Li_2[**1**] as a platform for the development of versatile hydrogenation catalysts. Our main group ambiphiles stand out for their ability to transfer not only one H_2 molecule to unsaturated compounds, but also two H^- ions to element halides. As key factors governing the catalyst performance, the B-bonded substituents and the counter cations have been identified. Mechanistic studies helped to confirm a concerted H_2 activation, explain the substrate scopes, and arrive at workable reaction conditions.

RESULTS AND DISCUSSION

The 9,10-dihydro-9,10-diboraanthracene (DBA) derivatives employed in this paper will be denoted as '**A**' whenever we refer to the general structure. Arabic numerals are assigned to species carrying specific B-bonded substituents (cf. Scheme 2). Aromatic dianion salts and their corresponding H_2-activation products are named M_2[**A**] and M_2[**A**-H_2], respectively (M^+ = Li^+, Na^+, K^+). The B-bonded substituents were chosen such that they cover a broad range of sizes (*e.g.*, H < Me < aryl) and group electronegativities (*e.g.*, alkyl < aryl < alkynyl).

Synthesis of DBAs A, Their Dianion Salts M_2[A], and Their H_2-Activation Products M_2[A-H_2]. The B-substituted DBAs **1**-**9** are accessible from 9,10-dibromo-DBA through (a) hydride transfer using Et_3SiH (**1**),[13] (b) nucleophilic substitution with LiC≡C*t*Bu (**2**),[8] (c) hydride transfer and subsequent hydroboration of HC≡C*t*Bu (**3**),[13] and (d) nucleophilic substitution with BrMgR (**4**-**9**; Scheme 2 top and the SI).[14–16] The *i*Pr derivative **6** underwent partial dehydroboration already during efforts at its purification by vacuum sublimation (110 °C, 10^{-3} mbar). Given that the H_2-activation reaction with Li_2[**1**] required temperatures of 100 °C,[8] compound **6** was regarded as too temperature sensitive to be considered further. All attempted reductions of **1**-**5** and **7**-**9** using Li metal, Na metal, or KC_8 in THF quantitatively furnished the corresponding dianion salts M_2[**1**]-M_2[**5**] and M_2[**7**]-M_2[**9**] with the only exception of the KC_8/**2** system (Scheme 2 bottom). H_2-activation reactions were successfully performed with all alkali metal salts compiled in Scheme 2 (bottom), apart from Li_2[**3**], which decomposed at the applied temperature of 100 °C, and Li_2[**9**], which showed no reaction due to steric hindrance.

In THF-d_8 solution, compound **9** possesses an ^{11}B NMR shift of 72 ppm,[15] as is typical of three-coordinate triarylboranes.[17] The sterically less shielded derivatives are characterized by ^{11}B signals in the ranges 43-40 ppm (**4**, **5**) and 38-36 ppm (**7**, **8**), at 33 ppm (**2**),[18] and 22 ppm (**1**), testifying to the presence of (weak) solvent adducts. Upon reduction, all resonances shift to higher field strengths (28-14 ppm). A successful H_2 addition is evidenced by doublet multiplicities of the ^{11}B signals and further upfield shifts to the region between –10 and –24 ppm. ^{1}H and ^{13}C{^{1}H} NMR spectra were recorded and assigned for all three substance classes **A**, M_2[**A**], and M_2[**A**-H_2]. The signal patterns are in agreement with the proposed structural motifs, which were also confirmed by X-ray analysis (cf. the SI for full details).

Scheme 2. Top: Synthesis of Symmetrically Substituted DBA Derivatives: a) Et_3SiH,[13] b) LiC≡C*t*Bu,[8] c) 1. Et_3SiH, 2. HC≡C*t*Bu,[13] d) RMgBr, Toluene/Et_2O, –78 °C to r.t. Bottom: Reduction of the DBA Derivatives with Alkali Metals; Reduction Successful (✓), Unsuccessful (✖), and not Investigated (–).

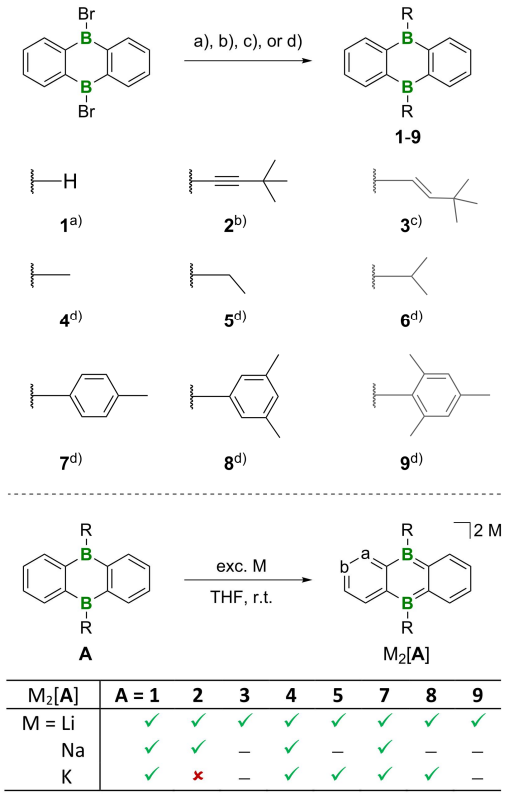

M_2[A]	A = 1	2	3	4	5	7	8	9
M = Li	✓	✓	✓	✓	✓	✓	✓	✓
Na	✓	✓	–	✓	–	✓	–	–
K	✓	✖	–	✓	✓	✓	✓	–

Key Parameters Determining the H_2 Activation with M_2[A]. *Influence of the B-bonded substituents:* The conversion of M_2[**A**] to M_2[**A**-H_2] leads to qualitatively similar changes in the ^{1}H NMR spectra of all derivatives **A** = **1**, **2**, **4**, **5**, **7**, **8**, which allowed us to monitor the reaction progress in dependence of the B-bonded substituents. We selected the Li_2[**A**] salts for this purpose in order to maximize the time resolution, knowing that Li_2[**1**] activates H_2 at a much slower rate than K_2[**1**].[8] All samples were prepared in flame-sealed NMR tubes and stored at 100 °C for several days (0.050 mmol Li_2[**A**], $p(H_2)$ < 1 atm at room temperature, THF-d_8). NMR spectra were recorded in regular intervals at room temperature with short measurement times and thus under conditions at which the reaction comes to a halt. The conversion-time diagram obtained reveals two important effects (Figure 1): 1. H_2 activation by the alkynyl derivative Li_2[**2**] cannot be driven to completion, but reaches a dynamic addition/elimination equilibrium.[8,19] 2. Smaller substituents result in faster H_2 addition

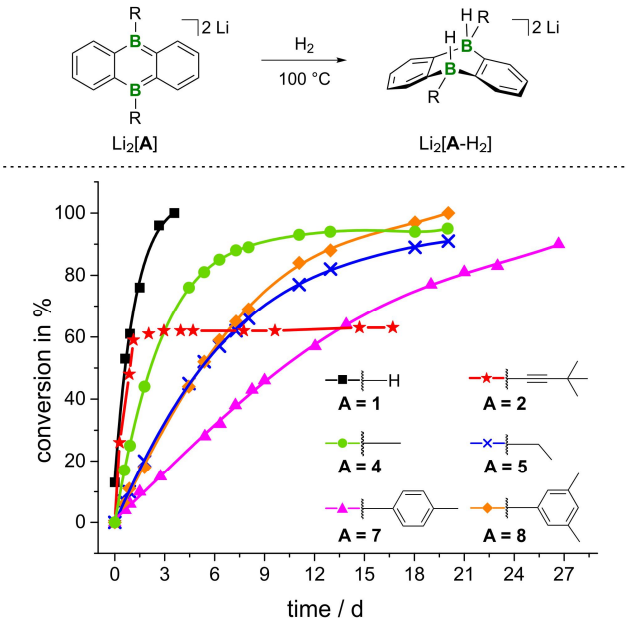

Figure 1. Conversion-time diagram for the reactions between Li_2[**A**] and H_2 to give Li_2[**A**-H_2] (obtained from ^{1}H NMR spectroscopy).

(cf. H, C≡C*t*Bu, Me *vs.* Et, *m*Xyl, *p*Tol). The latter finding can be rationalized by the fact that rapid H_2 addition requires unhindered access of the substrate molecule to the reactive boron sites. Barriers along the trajectory are the $[Li(thf)_n]^+$ ions, which form contact ion pairs with the negatively charged B_2C_4 heterocycles, not only in the solid state but also in THF solution.[8] By the same token, an increasing bulk of the substituent has a negative impact on the H_2 approach (kinetic control). One might argue that this effect could be compensated by a concomitant sterically induced weakening of the $Li^+\cdots$[**A**]$^{2-}$ interaction, but this assumption is not supported by X-ray crystallography: the average distances between Li^+ and the respective DBA centroids *decrease* rather than increase along the series $[Li(thf)_2]_2$[**1**] > $[Li(thf)_2]_2$[**4**] > $[Li(thf)_2]_2$[**7**] (1.960,[20] 1.911,[16] 1.891 Å, respectively).

Two questions are still remaining: 1. Why does the alkynyl species Li_2[**2**] show such a peculiar behavior? 2. Why is the performance of the sterically similar *p*Tol (Li_2[**7**]) and *m*Xyl (Li_2[**8**]) derivatives so different? We suggest the following answers based on the different stabilities of the [**A**]$^{2-}$ ions (a justification will be given below):[21] 1. Of all species Li_2[**A**], Li_2[**2**] contains the most stable dianion, which decreases the exoergicity of the H_2-addition reaction. At the same time, the high reaction velocity indicates an energetically low-lying transition state. Taken together, both factors render the forward as well as reverse reaction thermodynamically and kinetically feasible. 2. The stability of [**7**]$^{2-}$ is higher than that of [**8**]$^{2-}$. If we assume a closely similar steric contribution of the *p*Tol and *m*Xyl substituents to the kinetic shielding of the boron centers, the dianion [**8**]$^{2-}$ should be more reactive.

To a first approximation, the relative stabilities of the [**A**]$^{2-}$ ions are determined by the LUMO-energy levels of the neutral species **A** and, in turn, mirrored by the half-wave potentials $E_{1/2}$ of the **A**/[**A**]$^-$ redox couples (Figure 2). Due to its electronegative C(sp) substituents, compound **2** indeed possesses the least cathodic redox potential, followed by **7** and then **8** with less electronegative C(sp^2) aryl groups. Even harder to reduce are the C(sp^3) alkyl derivatives **4** and **5**. The reduction of the parent DBA **1** requires the most cathodic electrode potential, even though an H atom should be less electron releasing than, *e.g.*, an alkyl substituent. Yet, as evidenced by the ^{11}B NMR shifts mentioned above, **1** forms a strong THF adduct, which needs to be cleaved in the course of the reduction process and therefore hampers electron injection.[18] To further substantiate this interpretation, we also computed the LUMO energy levels of the DBAs (B3LYP/6-31G*). Now that THF ligation is not an issue, all LUMO energies, including that of **1**, follow the trend expected on the basis of electronic substituent effects (see the SI for more details).

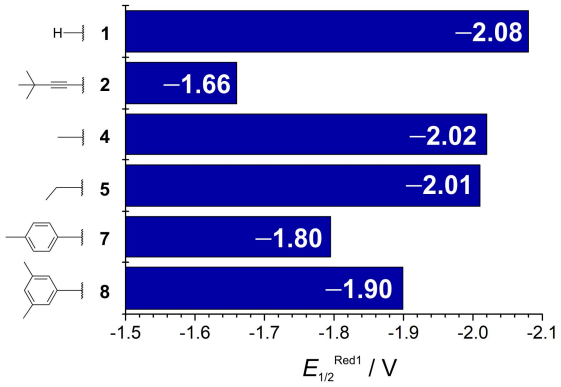

Figure 2. $E_{1/2}^{Red1}$ values of the compounds **1**, **2**, **4**, **5**, **7**, and **8** (THF, room temperature, supporting electrolyte [nBu$_4$N][PF_6], referenced against internal FcH/FcH^+).

Influence of the counter cations: As mentioned above, the formation of contact ion pairs in M_2[**A**] could impede the access of H_2 to the boron centers. It is generally accepted that the affinity of an alkali metal ion M^+ to the π face of an aryl ring follows an electrostatic trend and consequently decreases with an increasing ionic radius of M^+.[22] This is strictly true for the gas phase, but also applies for THF solutions of M_2[**A**]: ^{7}Li NMR spectroscopy on Li_2[**1**] provided evidence for the existence of contact ion pairs in THF-d_8 solution.[8] Corresponding information regarding the ion aggregation of Na_2[**1**] and K_2[**1**] was gained through $^{13}C\{^1H\}$ NMR spectroscopy. The peripheral *o*-phenylene carbon atom C-b is sensitive to changes in the π-electron structure of the B_2C_4 ring – a higher charge density leads to a higher magnetic shielding.[15] For Li_2[**1**], Na_2[**1**], and K_2[**1**], δ(C-b) equals to 118.3, 115.9, and 115.1 ppm, respectively. An M^+ cation located above the B_2C_4 plane should pull away charge density from the dianion and concomitantly cause a more downfield-shifted C-b signal. We therefore conclude that Na_2[**1**] and K_2[**1**] establish less strongly bound ion pairs than Li_2[**1**]. In line with that, THF solutions of Na_2[**1**] and K_2[**1**] possess a deep green color, whereas those of Li_2[**1**] are deep red. In the solid state, all three salts show the same structural motif of an inverse sandwich complex (Figure 3) and, in turn, exhibit the same dark red color. Given this background, the choice of M^+ could provide a similar powerful set-screw for tuning the reactivity of M_2[**A**] toward H_2 as the selection of the B-bonded substituent.

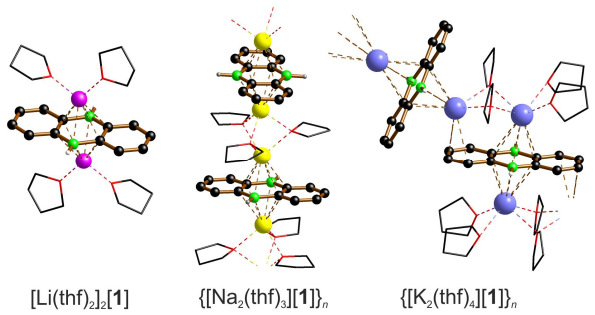

Figure 3. Solid-state structures of the discrete inverse-sandwich complex $[Li(thf)_2]_2[\mathbf{1}]$ and the coordination polymers $\{[Na_2(thf)_3][\mathbf{1}]\}_n$ and $\{[K_2(thf)_4][\mathbf{1}]\}_n$. C-bonded H atoms are omitted for clarity. Averaged $M^+\cdots$COG distances [Å]: Li^+ = 1.960, Na^+ = 2.239, K^+ = 2.755; COG = centroid of the planar B_2C_4 ring. A description of the crystal structures is provided in the SI.

To test this conclusion, we studied next the relative velocities of the H_2-activation reactions using $M^+ = Li^+$, Na^+, and K^+ in combination with the best performing dianions $[\mathbf{1}]^{2-}$, $[\mathbf{4}]^{2-}$ and the lowest performer $[\mathbf{7}]^{2-}$ (Figure 4). At a temperature of 100 °C, the Na^+ species react significantly faster than the Li^+ salts. A temperature decrease to 50 °C slows down the reaction rate of $Na_2[\mathbf{A}]$, whereas that of $K_2[\mathbf{A}]$ is still high, even in the case of the *p*Tol derivative $K_2[\mathbf{7}]$. All in all, a switch from $Li_2[\mathbf{A}]$ to $K_2[\mathbf{A}]$ cuts down the required reaction time from multiple days to few hours.

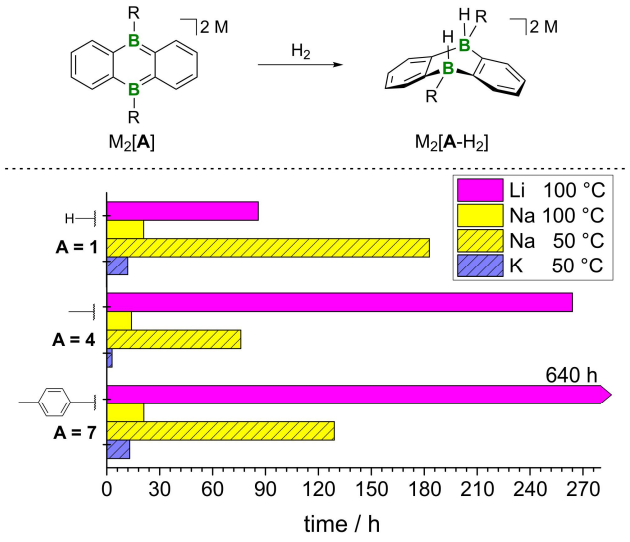

Figure 4. Velocity of the H_2 activation by $M_2[\mathbf{A}]$ as a function of the nature of the counter cation and the B-bonded substituent.

The H_2-activation products $Li_2[\mathbf{1}\text{-}H_2]$, $Na_2[\mathbf{7}\text{-}H_2]$, $K_2[\mathbf{1}\text{-}H_2]$, $K_2[\mathbf{4}\text{-}H_2]$, and $K_2[\mathbf{7}\text{-}H_2]$ have been investigated by X-ray analysis.[23] As a further counterion effect we note that $Li_2[\mathbf{1}\text{-}H_2]$ contains bent anions,[8] whereas the anion in $K_2[\mathbf{1}\text{-}H_2]$ is perfectly planar (Figure 5 left). Moreover, the inverse sandwich structure is retained, thereby allowing a direct comparison of the $K^+\cdots$COG distances before and after H_2 addition, which reveals a remarkably small increase of less than 6% (av. values: 2.755 *vs.* 2.917 Å; COG = centroid of the planar B_2C_4 ring). The other structurally characterized ions $[\mathbf{A}\text{-}H_2]^{2-}$ show bent frameworks. In agreement with a concerted, metal-like H_2-addition mechanism,[8] the B-bonded hydrogen atoms occupy axial positions of the boat-shaped B_2C_4 rings (*cis* configuration; cf. the structure of $[\mathbf{7}\text{-}H_2]^{2-}$ in Figure 5 right).

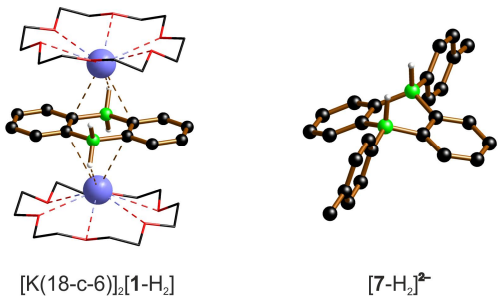

Figure 5. Solid-state structures of the discrete inverse-sandwich complex $[K(18\text{-c-}6)]_2[\mathbf{1}\text{-}H_2]$ (left) and a dianion of the dimeric $[Na][Na(thf)_2(18\text{-c-}6)][Na(thf)_2]_2(n\text{-hexane})[\mathbf{7}\text{-}H_2]_2$ (right). C-bonded H atoms are omitted for clarity.

Each of the lithium salts $Li_2[\mathbf{A}\text{-}H_2]$ shows one set of ^1H, ^{11}B, and $^{13}C\{^1H\}$ NMR signals. The same is true for $Na_2[\mathbf{1}\text{-}H_2]$ and $K_2[\mathbf{1}\text{-}H_2]$. In contrast, resonances assignable to two different, albeit closely related, products were observable after the quantitative conversion of $Na_2[\mathbf{4}]$, $Na_2[\mathbf{7}]$, $K_2[\mathbf{4}]$, or $K_2[\mathbf{7}]$ with H_2. A subsequent ^1H NMR monitoring of the $K_2[\mathbf{7}]/H_2$ mixture revealed one strongly predominant product in the early stages of the reaction (THF-d_8, 50 °C). Signals of a second product appeared as the reaction progressed and continuously gained intensity, even after full consumption of $K_2[\mathbf{7}]$ (Figure 6). The primary reaction product thus rearranges to the second product

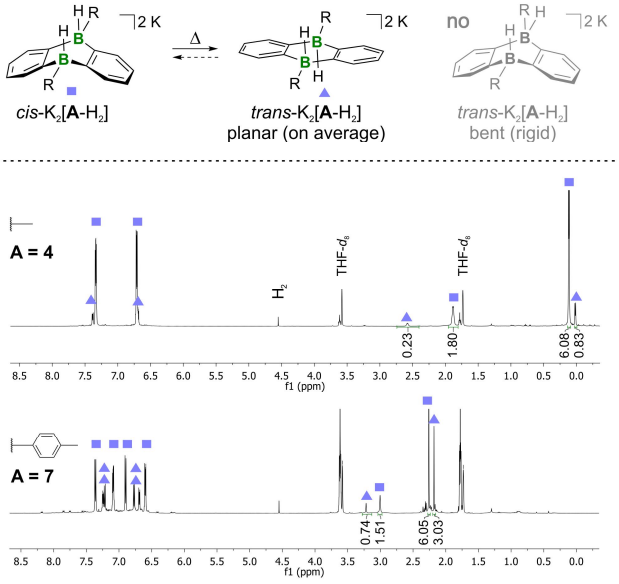

Figure 6. Thermally induced isomerization of the H_2-addition products $K_2[\mathbf{A}\text{-}H_2]$ (R = Me, *p*Tol). $^1H\{^{11}B\}$ NMR spectra (500.2 MHz, THF-d_8) of the reaction mixtures $K_2[\mathbf{4}]/H_2$ (top) and $K_2[\mathbf{7}]/H_2$ (bottom) after 13 h at 50 °C. The ratios between the *cis* (■) configuration (primary product of the H_2 addition) and the *trans* (▲) configuration (secondary product) depend on the B-bonded substituent.

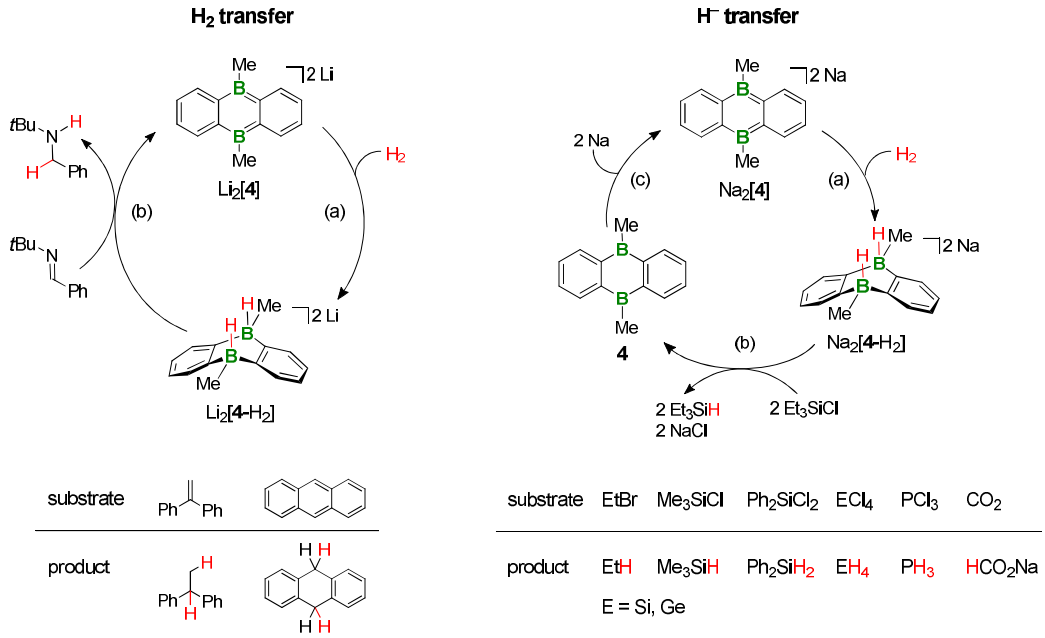

Figure 7. Left: Catalytic cycle for Li_2[**4**] as the hydrogenation catalyst. Right: Cyclic process for the transformation of Et_3SiCl into Et_3SiH with Na_2[**4**-H_2] as the hydride donor. (a) H_2 activation; (b) H_2/2H^- transfer; (c) DBA reduction.

at the elevated temperature applied. Since the NMR characteristics of the first as well as the second product point toward hydride diadducts of 9,10-(pTol)$_2$-DBA, the difference must lie in their *cis vs. trans* configurations.[24] Indeed, the THF-d_8 solution of manually selected single crystals of *cis*-Na_2[**7**-H_2] (confirmed by X-ray analysis; Figure 5 right) gave only one set of resonances (corresponding to those of the first product of the K_2[**7**]/H_2 reaction). During storage of the sample at 50 °C, a second signal set evolved (corresponding to that of the second product of the K_2[**7**]/H_2 reaction).

The nature of the primary hydrogenation products as *cis*-M_2[**A**-H_2] confirms the mechanistic picture of a concerted, metal-like H_2-addition reaction.[8] The single diastereomer observed for Li_2[**A**-H_2] is therefore the result of a completely kinetically controlled process where subsequent isomerization to the *trans* isomer is not taking place (in contrast to the Na^+ and K^+ counterparts). In this context, we also treated the DBA derivative **4** in THF-d_8 with 2 equiv of K[$HBEt_3$], which should react in a non-concerted fashion (LiH, NaH, and KH react only slowly due to solubility issues). This time, an equimolar mixture of *cis*/*trans*-K_2[**4**-H_2] was obtained (cf. the SI for more details).

The dianions *trans*-[**A**-H_2]$^{2-}$ must either be planar or invert rapidly on the NMR timescale, because otherwise they could not give rise to the highly symmetrical signal patterns observed (Figure 6).[25] In THF, the activities of alkali metal hydrides as rearrangement catalysts follow the order KH >> NaH > LiH,[26] which correlates with our observation that *cis*/*trans* isomerization is particularly pronounced for K_2[**7**-H_2], but not observed for Li_2[**7**-H_2]. We consequently propose dissociation/re-association of KH (or NaH) as key isomerization step. Apart from the counter cation, also the B-bonded substituent influences the *cis*/*trans* isomerization as evidenced by the fact that *cis*-K_2[**7**-H_2] rearranges to a larger extent than *cis*-K_2[**4**-H_2] (Figure 6).

Dual Role of M_2[A-H_2] as H_2- and H^--Transfer Catalysts. FLPs are nowadays established hydrogenation catalysts, because they are capable not only of activating H_2 but also of transferring it onto a plethora of substrates. The observation that Li_2[**2**-H_2] liberates the added H_2 even in the absence of an acceptor molecule suggests similarly useful applications for main group ambiphiles M_2[**A**], too. Alternatively, M_2[**A**-H_2] could supply *two H⁻ ions*, which decidedly distinguishes them from classical FLPs, because the latter heterolytically cleave H_2 to furnish only one H^- ion together with a proton. Based on these considerations, we propose a dual role of the M_2[**A**]/M_2[**A**-H_2] system both for the conversion of unsaturated into saturated compounds (Figure 7 left) and the transformation of element–halogen into element–hydrogen bonds (Figure 7 right). After successful H_2 transfer, M_2[**A**] is regenerated in an inherently catalytic process. The transfer of two H^- ions, however, leaves the neutral DBA behind, which needs to be recharged with two electrons before it can activate a new H_2 molecule and enter the cycle again.

H_2 transfer: For start, we discuss the scope and limitations of selected M_2[**A**] derivatives as hydrogenation catalysts. The system was optimized with regard to the counter cation (M^+ = Li^+, Na^+, or K^+) and the B-bonded substituent (H, Me, or pTol) by using the imine Ph(H)C=NtBu as the model substrate (catalyst loading: 37mol%, 1 atm H_2, THF, 100 °C, 16 h; Table 1).

Table 1. Percent Conversion of the Imine Ph(H)C=N*t*Bu to its Hydrogenation Product Ph(H)$_2$C–N(H)*t*Bu Using Nine Different M_2[A] Combinations (Catalyst Load: 37mol%, 1 atm H_2, THF, 100 °C, 16 h).

[A]$^{2-}$ derivative	$M^+ = Li^+$	$M^+ = Na^+$	$M^+ = K^+$
M_2[**1**]	11	1	1
M_2[**4**]	97	27	1
M_2[**7**]	3	0	0

Irrespective of the choice of $[\mathbf{A}]^{2-}$, Li^+ performed much better than its higher homologs. The cation trend observed for the overall catalytic process (cf. entry 2) is in fact inverse to that observed for the H_2-activation step alone (see above). Even though strong contact ion pair formation has an adverse effect on the H_2 addition, it provides the necessary thrust for the H_2 transfer from Li_2[**A**-H_2] by thermodynamically stabilizing the liberated Li_2[**A**] (cf. the H_2 addition/elimination equilibrium observed for the particularly stable Li_2[**2**]). Apparently, the beneficial influence of Li^+ coordination on the second step outweighs its negative impact on the first step.

Of the three B-bonded substituents studied, *p*Tol turned out to be least suitable, likely because it exerts a high steric hindrance not only on H_2 addition, but also on its transfer. The smaller Me substituent gave excellent results, but a further decrease in substituent size from Me to H led to a less active catalyst again. We assumed the origin behind this puzzling finding was a [4+2]-cycloaddition reaction between Ph(H)C=N*t*Bu and Li_2[**1**], which competes with H_2 activation and poisons the catalyst. Such reactivity has its precedence in cycloadditions between Li_2[**1**] or Li_2[**4**] and carbonyl

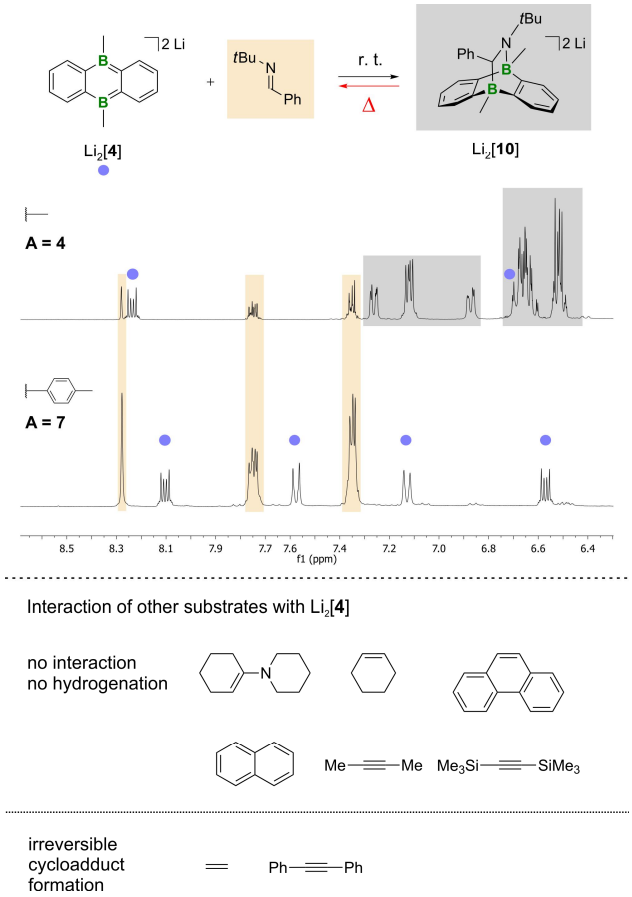

Figure 8. Top: Comparison of the interaction between Li_2[**A**] and Ph(H)C=N*t*Bu in dependence of the B-bonded substituents R = Me or *p*Tol. The ^{1}H NMR spectra of respective 1:1 mixtures were recorded immediately after sample preparation (500.2 MHz, THF-d_8). Bottom: Some substrates form irreversible [4+2]-cycloaddition products with Li_2[**4**], whereas others show no interaction.

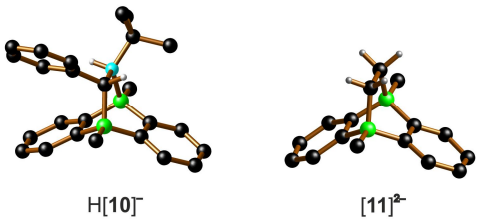

Figure 9. Solid-state structures of the anions of [Li(12-c-4)$_2$]H[**10**]·THF (left) and [Li(12-c-4)(thf)][Li(12-c-4)][**11**] (right). Most C-bonded H atoms are omitted for clarity.

compounds.[16, 20] NMR spectra recorded on equimolar mixtures of Ph(H)C=N*t*Bu and Li_2[**1**] or Li_2[**4**] showed signals assignable to the expected tricyclic skeletons, *i.e.*, ^{1}H-, ^{11}B-, and ^{13}C-signal patterns indicative of C_1-symmetric DBA fragments, proton-integral ratios in line with 1:1 cycloadducts, and ^{11}B resonances typical of four-coordinate boron centers (cf. Figure 8). Moreover, the cycloadduct Li_2[**10**] of Li_2[**4**] was structurally characterized by X-ray diffraction, albeit only in its *N*-protonated form [Li(12-c-4)$_2$]H[**10**] (Figure 9). We speculate that the crown ether-induced ion separation led to a significantly enhanced basicity of the N atoms, which therefore abstracted protons from adventitious traces of water during the prolonged crystallization process (cf. the SI for more information). In the case of Li_2[**1**], cycloadduct formation is fast and quantitative already at room temperature; Li_2[**4**] reacts at a much slower rate such that the NMR resonances of the two starting materials and the product Li_2[**10**] are detectable at the same time (Figure 8). At 100 °C, the temperature required for imine hydrogenation, Li_2[**10**] reverts back to a much higher degree than the corresponding Li_2[**1**] cycloadduct, which straightforwardly explains the observed differences in the catalytic activities of Li_2[**4**] *vs.* Li_2[**1**]. We finally note that the *p*Tol derivative Li_2[**7**] shows no interaction with Ph(H)C=N*t*Bu (Figure 8).

Having identified Li_2[**4**] as the best performing catalyst, we next confirmed that its loading can be cut down from the previously employed 37mol% to 10mol% without detrimental consequences on product yield and conversion time. As a proof-of-principle, the reaction was also conducted in a 100 mL stainless steel autoclave to prepare 150 mg of Ph(H)$_2$C–N(H)*t*Bu (catalyst loading: 10mol%, 7 bar H_2, THF, 100 °C, 18 h). To obtain a first impression of the substrate scope, we selected the 10 unsaturated compounds compiled in Figures 7 and 8. Of these species, which contain either C=C double or C≡C triple bonds and differ in their steric and electronic properties, $Ph_2C=CH_2$ and anthracene underwent quantitative hydrogenation. The remaining substrates that failed to be hydrogenated can be categorized in two groups: Members of the first group behave entirely inert toward Li_2[**4**]/H_2, whereas those of the second group form stable [4+2]-cycloadducts with the $[\mathbf{4}]^{2-}$ ion (for a crystallographic proof of the formation of the ethylene cycloadduct Li_2[**11**] see Figure 9).[27] For a successful hydrogenation, one has therefore to maintain a delicate balance between the steric demands of the catalyst and the substrate molecules.

Apart from steric influences also electronic factors likely govern the substrate scope. The Woodward-Hoffmann rules predict that the metal-like addition of an unpolar H–H bond across the boron atoms of M_2[**A**] proceeds via a thermally

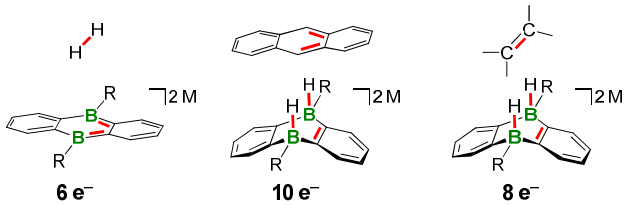

Figure 10. Illustration of the concerted H_2 activation with M_2[**A**] (allowed; left) and the H_2 transfers from M_2[**A**-H_2] to either anthracene (allowed; middle) or an olefin (forbidden; right).

allowed transition state (6 e^-; Figure 10).[8] The concerted H_2 transfer from M_2[**A**-H_2] to anthracene is also allowed (10 e^-), but forbidden for olefins and alkynes (8 e^-).[28] Related issues have already been discussed for the established H_2-donor reagent 9,10-dihydroanthracene, an isoelectronic neutral analog of [**A**]$^{2-}$.[29] Here it is generally accepted that the reactions follow two-step mechanisms, either involving initial H^--ion or $H^\bullet$-atom transfer.[30] The lower electronegativity of boron compared to carbon results in a more negative partial charge on the bridgehead hydrogen atoms of [**A**-H_2]$^{2-}$ than on those of 9,10-dihydroanthracene. An ionic pathway should therefore be favored in our case – also considering that we never observed indications for the presence of paramagnetic intermediates or byproducts during *in situ* NMR experiments (*e.g.*, deuterium abstraction from THF-d_8, unusual signal broadening).[31] The assumption of an initial H^--ion transfer straightforwardly explains why [**4**-H_2]$^{2-}$ failed to hydrogenate the enamine 1-(1-piperidinyl)cyclohexene, an archetypal substrate in FLP-reduction chemistry: Classical FLPs usually transfer an H^+ ion first and after an H^- ion and consequently prefer electron-rich reaction partners,[10] whereas the opposite should be true for [**4**-H_2]$^{2-}$. To further substantiate this interpretation, we treated Na_2[**4**-H_2] with 1 equiv of Et_3SiCl and quantitatively obtained Et_3SiH together with Na[**4**-H], a monoanion salt with only one remaining bridgehead hydrogen (cf. the SI and Ref.[32]). This experiment also lays the conceptual foundation for the use of [**A**-H_2]$^{2-}$ as a source of two H^- nucleophiles, which is discussed in the next paragraph.

H^- transfer: The transformation of element halides into element hydrides was optimized with the help of Et_3SiCl as the model substrate. Contrary to the case of the hydrogenation reaction, a twofold H^--transfer from [**A**-H_2]$^{2-}$ liberates the catalyst molecule in its spent neutral state **A**. A circular process thus requires the re-reduction of **A** to [**A**]$^{2-}$ in the absence of Et_3SiCl to avoid unwanted Wurtz-type coupling of the chlorosilane.[33] The resulting necessity for a temporal separation of the alkali metal reduction and H_2-activation steps from the H/Cl-exchange step demands an alternating addition of the three components to the catalyst system. Before the stoichiometric amount of Et_3SiCl is allowed into the reaction vessel, the formation of [**A**-H_2]$^{2-}$ has to be quantitative and should therefore proceed as fast as possible, which renders Na metal or KC_8 the reducing agents of choice. Considering safety hazards and the higher lattice energy of NaCl compared to KCl,[34] we identified Na_2[**4**] as the best-suited catalyst system for the given purpose. It has to be emphasized that an alternating process management is not uncommon even on an industrial scale, a famous example being the anthraquinone process for the production of H_2O_2.[35]

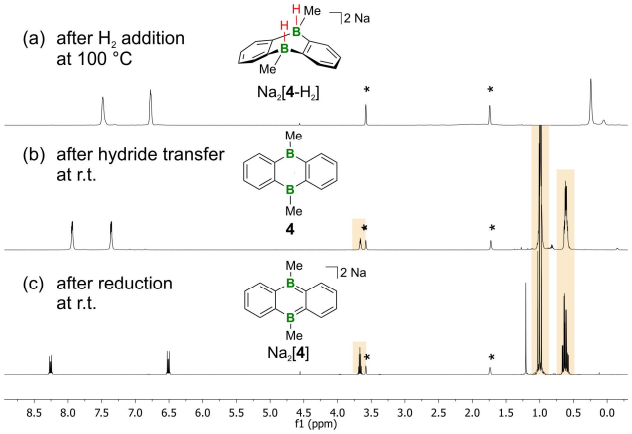

Figure 11. ^{1}H NMR spectra (400.0, 500.2 MHz; THF-d_8) recorded after each step of the catalytic cycle shown in Figure 7 right; the reaction product Et_3SiH is highlighted in beige; residual solvent resonances are marked with (*).

Figure 11 shows ^{1}H NMR spectra recorded after each of the three reaction steps required to complete a full cycle. The individual conversions, carried out at 100 °C (H_2 activation) or room temperature (H/Cl exchange; re-reduction of **4**), are quantitative and perfectly selective with no detectable formation of side products. The product Et_3SiH does not interfere with any of the subsequent steps and can therefore be accumulated over multiple cycles (a corresponding proof-of-principle experiment is outlined in the SI). As discussed above, the alternating process management is enforced by the fact that the reduction of **4** has to be carried out separately from the H^--transfer reaction to circumvent wasting starting materials through unwanted Si–Si coupling. Yet, in the course of our studies we discovered an even more pressing reason that directly affects the integrity of the catalyst: The electron-rich [**4**]$^{2-}$ acts as a remarkable boron-centered nucleophile[36] toward Et_3SiCl and furnishes the monoanionic silylborate [MeB-(oC$_6$H$_4$)$_2$-B(Me)SiEt$_3$]$^-$ containing one four-coordinate boron atom with a B–Si bond (cf. the SI for more information).

The H/halogen-exchange reaction works faithfully not only for other tetrel halides, but also for PCl_3 as an example of the pnictogen halides (Figure 7 right). A mere H^- addition to give sodium formate was achieved for CO_2.[37] So far, we encountered no substrate limitations for Na_2[**4**-H_2] as a H^- source, however, investigations are still ongoing. With the help of Me_2SiCl_2, we next addressed the question: Are partially hydrogenated products available if the number of halide substituents in the substrate molecules exceeds the number of provided H^- ions? ^{1}H and ^{29}Si NMR spectroscopy on a 1:2 mixture of Na_2[**4**-H_2] and Me_2SiCl_2 revealed equimolar amounts of unreacted starting material (Me_2SiCl_2) and dimethylsilane (Me_2SiH_2) immediately after sample preparation. Over time, new resonances slowly grew in that were assignable to dimethylchlorosilane ($Me_2Si(H)Cl$; Scheme 3). The comproportionation reaction becomes significantly faster with increasing temperature (120 °C) and is mediated by the Lewis acidic borane **4**.[38] Thus, the DBA serves two purposes in the overall process, first to accomplish H_2 activation/H^- transfer and second to catalyze the silane comproportionation. The obtained $Me_2Si(H)Cl$ is a most important building block for the silicone

Scheme 3. 1 Equiv Me_2SiCl_2 is Quantitatively Converted to 1 Equiv Me_2SiH_2 Upon Treatment with 1 Equiv Na_2[4-H_2]. If an Excess of Me_2SiCl_2 is Present, the Lewis Acid 4 Catalyzes a Subsequent Dismutation Reaction Furnishing 2 Equiv $Me_2Si(H)Cl$.

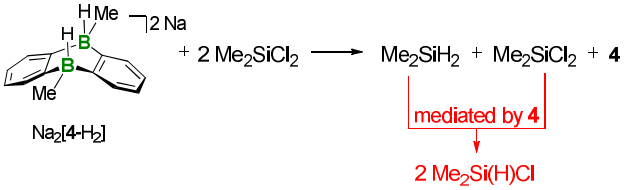

industry, because it possesses two orthogonal reactive sites and can extensively be derivatized via hydrosilylation protocols.[39]

It has been proposed that the reduction of chlorosilanes with aluminium hydrides involves four-membered Al-H-Si-Cl rings in the transition state.[40] A similar scenario is also conceivable for [**4**-H_2]$^{2-}$ as the reducing agent. Alternatively, a chlorosilane R_3SiCl could abstract one H^- ion from Na_2[**4**-H_2] (or Na[**4**-H]) to afford Na[$R_3Si(H)Cl$] and Na[**4**-H] (or **4**). The subsequent elimination of NaCl from the five-coordinate Na[$R_3Si(H)Cl$] should be facile. The comproportionation reaction Me_2SiH_2 + Me_2SiCl_2 → 2 $Me_2Si(H)Cl$ catalyzed by **4** likely starts with the formation of an adduct $R_3B\cdots H–Si(H)Me_2$. Such intermediates, which have already been described in the context of triorganylborane-mediated hydrosilylation and Piers-Rubinsztajn reactions,[41] are prone to nucleophilic attack at the silicon atom. If the incoming nucleophile is a chlorine substituent of Me_2SiCl_2, the formation of a disilyl chloronium salt [R_3BH][$Me_2(H)Si–Cl–Si(Cl)Me_2$] can be envisaged.[42] H^- migration from boron to silicon finally affords 2 equiv of $Me_2Si(H)Cl$.

CONCLUSION

The ambiphilic doubly reduced 9,10-dihydro-9,10-diboraanthracenes $[DBA]^{2-}$ described in this paper have taken the next step in mimicking transition metal complexes, because they not only activate H_2 but can subsequently use both hydrogen atoms for further syntheses. Depending on the specific substrate, the transfer of the H_2 equivalent either results in the hydrogenation of unsaturated bonds (formal delivery of an H^+ and H^- ion) or in the nucleophilic substitution at E–X bonds (delivery of two H^- ions). If in the latter case the released neutral DBA is re-reduced, it can run through the process again and thereby act as a rechargeable analog of $NaBH_4$.

For the H_2-activation step alone, it is advantageous to select a weakly coordinating counter cation and a small B-bonded substituent in order to minimize steric hindrance to the approaching H_2 molecule. An opposite counter cation effect is operative for the H_2-transfer step, because cation coordination stabilizes the regenerated $[DBA]^{2-}$ dianion. Moreover, the B-bonded substituent must not be too small to avoid catalyst poisoning through the formation of persistent substrate-$[DBA]^{2-}$ cycloadducts. H^- transfer proved less sensitive to the choices of the B-bonded substituents and the cations, such that the focus can be placed on maximizing the efficiency of the H_2-activation step. We finally came to the result that Li_2[**4**] and Na_2[**4**] carrying Me groups at boron are best suited to mediate H_2- and double H^--transfer reactions, respectively.

We have shown in the past that a derivatization of the DBA scaffold is also facile at the *o*-phenylene rings.[43] Almost any substitution pattern can be installed, which allows the preparation of custom-tailored catalysts. Yet, the largest potential for further improvement arguably lies in the replacement of the alkali metal reductants by an electric current to close the catalytic H^--transfer cycle.

ASSOCIATED CONTENT

Supporting Information.

The Supporting Information is available free of charge on the ACS Publications website at DOI: 10.1021/jacs.xxxxxxx.

Experimental details and characterization data (PDF)
X-ray crystallographic data (CIF)
Cartesian coordinates of calculated structures (XYZ)

AUTHOR INFORMATION

Corresponding Author

* matthias.wagner@chemie.uni-frankfurt.de

Notes

The authors declare no competing financial interest.

ACKNOWLEDGMENT

The authors gratefully acknowledge Dr. Thomas Kaese and Marc Zeplichal (M.Sc.) for their assistance with quantum chemical calculations and autoclave experiments, respectively.

REFERENCES

(1) (a) Erker, G.; Stephan, D. W. (Eds.), *Frustrated Lewis Pairs I & II*, Springer, Heidelberg, **2013**; (b) Stephan, D. W.; Erker, G., Frustrated Lewis Pair Chemistry of Carbon, Nitrogen and Sulfur Oxides. *Chem. Sci.* **2014**, *5*, 2625; (c) Stephan, D. W., Frustrated Lewis Pairs. *J. Am. Chem. Soc.* **2015**, *137*, 10018.

(2) (a) Chu, T.; Nikonov, G. I., Oxidative Addition and Reductive Elimination at Main-Group Element Centers. *Chem. Rev.* **2018**, *118*, 3608; (b) Weetman, C.; Inoue, S., The Road Travelled: After Main-Group Elements as Transition Metals. *Chem. Cat. Chem* **2018**, *10*, 4213; (c) Hadlington, T. J.; Driess, M.; Jones, C., Low-Valent Group 14 Element Hydride Chemistry: Towards Catalysis. *Chem. Soc. Rev.* **2018**, *47*, 4176; (d) Dagorne, S.; Wehmschulte, R., Recent Developments on the Use of Group 13 Metal Complexes in Catalysis. *Chem. Cat. Chem.* **2018**, *10*, 2509; (e) Légaré, M.-A.; Pranckevicius, C.; Braunschweig, H., Metallomimetic Chemistry of Boron. *Chem. Rev.* **2019**, DOI: 10.1021/acs.chemrev.8b00561.

(3) Dahcheh, F.; Martin, D.; Stephan, D. W.; Bertrand, G., Synthesis and Reactivity of a CAAC-Aminoborylene Adduct: A Hetero-Allene or an Organoboron Isoelectronic with Singlet Carbenes. *Angew. Chem. Int. Ed.* **2014**, *53*, 13159.

(4) (a) Peng, Y.; Guo, J. D.; Ellis, B. D.; Zhu, Z.; Fettinger, J. C.; Nagase, S.; Power, P. P., Reaction of Hydrogen or Ammonia with Unsaturated Germanium or Tin Molecules under Ambient Conditions: Oxidative Addition versus Arene Elimination. *J. Am. Chem. Soc.* **2009**, *131*, 16272; (b) Seifert, A.; Scheid, D.; Linti, G.; Zessin, T., Oxidative Addition Reactions of Element–Hydrogen Bonds with Different Polarities to a Gallium(I) Compound. *Chem. Eur. J.* **2009**, *15*, 12114; (c) Martin, D.; Soleilhavoup, M.; Bertrand, G., Stable Singlet Carbenes as Mimics for Transition Metal Centers. *Chem. Sci.* **2011**, *2*, 389; (d) Protchenko, A. V.; Birjkumar, K. H.; Dange, D.;

Schwarz, A. D.; Vidovic, D.; Jones, C.; Kaltsoyannis, N.; Mountford, P.; Aldridge, S., A Stable Two-Coordinate Acyclic Silylene. *J. Am. Chem. Soc.* **2012**, *134*, 6500; (e) Chu, T.; Korobkov, I.; Nikonov, G. I., Oxidative Addition of Sigma Bonds to an Al(I) Center. *J. Am. Chem. Soc.* **2014**, *136*, 9195; (f) Protchenko, A. V.; Bates, J. I.; Saleh, L. M.; Blake, M. P.; Schwarz, A. D.; Kolychev, E. L.; Thompson, A. L.; Jones, C.; Mountford, P.; Aldridge, S., Enabling and Probing Oxidative Addition and Reductive Elimination at a Group 14 Metal Center: Cleavage and Functionalization of E–H Bonds by a Bis(boryl)stannylene. *J. Am. Chem. Soc.* **2016**, *138*, 4555.

(5) Tsukahara, N.; Asakawa, H.; Lee, K. H.; Lin, Z.; Yamashita, M., Cleaving Dihydrogen with Tetra(*o*-tolyl)diborane(4). *J. Am. Chem. Soc.* **2017**, *139*, 2593.

(6) (a) Zhu, Z.; Wang, X.; Peng, Y.; Lei, H.; Fettinger, J. C.; Rivard, E.; Power, P. P., Addition of Hydrogen or Ammonia to a Low-Valent Group 13 Metal Species at 25 °C and 1 Atmosphere. *Angew. Chem. Int. Ed.* **2009**, *48*, 2031; (b) Fan, C.; Mercier, L. G.; Piers, W. E.; Tuononen, H. M.; Parvez, M., Dihydrogen Activation by Antiaromatic Pentaarylboroles. *J. Am. Chem. Soc.* **2010**, *132*, 9604; (c) Li, J.; Schenk, C.; Goedecke, C.; Frenking, G.; Jones, C., A Digermyne with a Ge–Ge Single Bond That Activates Dihydrogen in the Solid State. *J. Am. Chem. Soc.* **2011**, *133*, 18622; (d) Hermann, M.; Goedecke, C.; Jones, C.; Frenking, G., Reaction Pathways for Addition of H_2 to Amido-Ditetrylynes $R_2N–EE–NR_2$ (E = Si, Ge, Sn). A Theoretical Study. *Organometallics* **2013**, *32*, 6666; (e) Hadlington, T. J.; Jones, C., A Singly Bonded Amido-Distannyne: H_2 Activation and Isocyanide Coordination. *Chem. Commun.* **2014**, *50*, 2321; (f) Arrowsmith, M.; Böhnke, J.; Braunschweig, H.; Celik, M. A.; Dellermann, T.; Hammond, K., Uncatalyzed Hydrogenation of First-Row Main Group Multiple Bonds. *Chem. Eur. J.* **2016**, *22*, 17169; (g) Nagata, K.; Murosaki, T.; Agou, T.; Sasamori, T.; Matsuo, T.; Tokitoh, N., Activation of Dihydrogen by Masked Doubly Bonded Aluminum Species. *Angew. Chem. Int. Ed.* **2016**, *55*, 12877; (h) Araki, T.; Hirai, M.; Wakamiya, A.; Piers, W. E.; Yamaguchi, S., Antiaromatic Dithieno-1,2-dihydro-1,2-diborin Splits Diatomic Hydrogen. *Chem. Lett.* **2017**, *46*, 1714; (i) Wendel, D.; Szilvási, T.; Jandl, C.; Inoue, S.; Rieger, B., Twist of a Silicon–Silicon Double Bond: Selective *Anti*-Addition of Hydrogen to an Iminodisilene. *J. Am. Chem. Soc.* **2017**, *139*, 9156.

(7) (a) Taylor, J. W.; McSkimming, A.; Guzman, C. F.; Harman, W. H., N-Heterocyclic Carbene-Stabilized Boranthrene as a Metal-Free Platform for the Activation of Small Molecules. *J. Am. Chem. Soc.* **2017**, *139*, 11032; (b) Su, Y.; Li, Y.; Ganguly, R.; Kinjo, R., Engineering the Frontier Orbitals of a Diazadiborinine for Facile Activation of H_2, NH_3, and an Isonitrile. *Angew. Chem. Int. Ed.* **2018**, *57*, 7846.

(8) von Grotthuss, E.; Diefenbach, M.; Bolte, M.; Lerner, H.-W.; Holthausen, M. C.; Wagner, M., Reversible Dihydrogen Activation by Reduced Aryl Boranes as Main-Group Ambiphiles. *Angew. Chem. Int. Ed.* **2016**, *55*, 14067.

(9) (a) Welch, G. C.; San Juan, R. R.; Masuda, J. D.; Stephan, D. W., Reversible, Metal-Free Hydrogen Activation. *Science* **2006**, *314*, 1124; (b) Frey, G. D.; Lavallo, V.; Donnadieu, B.; Schoeller, W. W.; Bertrand, G., Facile Splitting of Hydrogen and Ammonia by Nucleophilic Activation at a Single Carbon Center. *Science* **2007**, *316*, 439; (c) Power, P. P., Main-Group Elements as Transition Metals. *Nature* **2010**, *463*, 171; (d) Zhao, L.; Huang, F.; Lu, G.; Wang, Z.-X.; Schleyer, P., Why the Mechanisms of Digermyne and Distannyne Reactions with H_2 Differ So Greatly. *J. Am. Chem. Soc.* **2012**, *134*, 8856.

(10) Stephan, D. W., "Frustrated Lewis Pair" Hydrogenations. *Org. Biomol. Chem.* **2012**, *10*, 5740.

(11) For a remote example see: Abdalla, J. A.; Riddlestone, I. M.; Tirfoin, R.; Aldridge, S., Cooperative Bond Activation and Catalytic Reduction of Carbon Dioxide at a Group 13 Metal Center. *Angew. Chem. Int. Ed.* **2015**, *54*, 5098.

(12) Hinz, A.; Schulz, A.; Villinger, A., Metal-Free Activation of Hydrogen, Carbon Dioxide, and Ammonia by the Open-Shell Singlet Biradicaloid [P(μ-NTer)]$_2$. *Angew. Chem. Int. Ed.* **2016**, *55*, 12214. Reversible H_2 activation by a triphosphabenzene has also been published: Longobardi, L. E.; Russell, C. A.; Green, M.; Townsend, N. S.; Wang, K.; Holmes, A. J.; Duckett, S. B.; McGrady, J. E.; Stephan, D. W., Hydrogen Activation by an Aromatic Triphosphabenzene. *J. Am. Chem. Soc.* **2014**, *136*, 13453.

(13) Lorbach, A.; Bolte, M.; Li, H.; Lerner, H.-W.; Holthausen, M. C.; Jäkle, F.; Wagner, M., 9,10-Dihydro-9,10-diboraanthracene: Supramolecular Structure and Use as a Building Block for Luminescent Conjugated Polymers. *Angew. Chem. Int. Ed.* **2009**, *48*, 4584.

(14) (a) Eisch, J. J.; Kotowicz, B. W., Novel Organoborane Lewis Acids via Selective Boron-Tin Exchange Processes Steric Constraints to Electrophilic Initiation by the Boron Halide. *Eur. J. Inorg. Chem.* **1998**, *1998*, 761; (b) Kessler, S. N.; Neuburger, M.; Wegner, H. A., Bidentate Lewis Acids for the Activation of 1,2-Diazines - a New Mode of Catalysis. *Eur. J. Org. Chem.* **2011**, 3238.

(15) Hoffend, C.; Diefenbach, M.; Januszewski, E.; Bolte, M.; Lerner, H.-W.; Holthausen, M. C.; Wagner, M., Effects of Boron Doping on the Structural and Optoelectronic Properties of 9,10-Diarylanthracenes. *Dalton Trans.* **2013**, *42*, 13826.

(16) von Grotthuss, E.; Prey, S. E.; Bolte, M.; Lerner, H.-W.; Wagner, M., Selective CO_2 Splitting by Doubly Reduced Aryl Boranes to Give CO and $[CO_3]^{2-}$. *Angew. Chem. Int. Ed.* **2018**, *57*, 16491.

(17) Nöth, H.; Wrackmeyer, B., *Nuclear Magnetic Resonance Spectroscopy of Boron Compounds*, in *NMR Basic Principles and Progress* (Eds.: P. Diehl, E. Fluck, R. Kosfeld), Springer: Berlin, **1978**.

(18) In **2**, the boron atoms are located in the shielding cone of the C≡C triple bond (cf. $\delta(^{11}B)$ in C_6D_6: **2** = 53 ppm, **9** = 73 ppm). Care must be taken not to overestimate the extent of THF ligation in **2** on the basis of the $\delta(^{11}B)$ value recorded for this compound in THF-d_8. We therefore believe that THF ligation is mainly relevant for **1** (and here for its redox potential).

(19) Also for the Me derivative **4**, a dynamic equilibrium close to 90% conversion cannot be excluded, but the size of the effect is likely already beyond the limits of measurement error.

(20) Lorbach, A.; Bolte, M.; Lerner, H.-W.; Wagner, M., Dilithio 9,10-diborataanthracene: Molecular Structure and 1,4-Addition Reactions. *Organometallics* **2010**, *29*, 5762.

(21) The conversion of the sodium salt Na_2[**2**] to Na_2[**2**-H_2] is quantitative after 93 h at 100 °C. Thus, not only the stability of the $[\mathbf{2}]^{2-}$ ion but also the nature of the counter cation is an important factor.

(22) (a) Kumpf, R. A.; Dougherty, D. A., A Mechanism for Ion Selectivity in Potassium Channels: Computational Studies of Cation-π Interactions. *Science* **1993**, *261*, 1708; (b) Ma, J. C.; Dougherty, D., The Cation−π Interaction. *Chem. Rev.* **1997**, *97*, 1303; (c) Gokel, G. W.; De Wall, S. L.; Meadows, E. S., Experimental Evidence for Alkali Metal Cation−π Interactions. *Eur. J. Org. Chem.* **2000**, 2967; (d) Ilkhechi, A. H.; Mercero, J. M.; Silanes, I.; Bolte, M.; Scheibitz, M.; Lerner, H.-W.; Ugalde, J. M.; Wagner, M., A Joint Experimental and Theoretical Study of Cation-π Interactions: Multiple-Decker Sandwich Complexes of Ferrocene with Alkali Metal Ions (Li^+, Na^+, K^+, Rb^+, Cs^+). *J. Am. Chem. Soc.* **2005**, *127*, 10656; (e) Kaufmann, L.; Vitze, H.; Bolte, M.; Lerner, H.-W.; Wagner, M., Experimental Assessment of the Relative Affinities of Benzene and Ferrocene toward the Li^+ Cation. *Organometallics* **2007**, *26*, 1771.

(23) The compounds crystallize as (dimeric) solvates [Li(thf)$_2$][Li(thf)][**1**-H_2], [Na][Na(thf)$_2$(18-c-6)][Na(thf)$_2$]$_2$(*n*-hexane)[**7**-H_2]$_2$, [K(18-c-6)]$_2$[**1**-H_2], [K][K(thf)]$_3$[**4**-H_2]$_2$, and [K]$_2$[K(18-c-6)][K(18-c-6)(thf)$_2$][**7**-H_2]$_2$. A discussion of the crystal structures is provided in the SI.

(24) For a related, BH_3·SMe_2 mediated *cis*/*trans* isomerization of a hydrogenated 1,4,2,5-diazadiborinine, see: Wang, B.; Kinjo, R., Activation of Dihydrogen by 1,4,2,5-Diazadiborinine. *Tetrahedron* **2018**, *74*, 7273.

(25) A planar configuration was also observed for the pyridine diadduct of the parent DBA **1**, see Ref. [13].

(26) Slaugh, L. H., Metal Hydrides. Hydrogenation and Isomerization Catalysts. *J. Org. Chem.* **1967**, *32*, 108.

(27) For a related ethylene cycloaddition product of 1,3,2,5-diazadiborinine, see: Wu, D.; Ganguly, R.; Li, Y.; Hoo, S. N.; Hirao, H.; Kinjo, R., Reversible [4+2] Cycloaddition Reaction of 1,3,2,5-Diazadiborinine with Ethylene. *Chem. Sci.* **2015**, *6*, 7150.

(28) In principle, a thermally allowed 6 e^- transition state would be achievable also for olefins and alkynes if we assume that a Dewar benzene-like valence isomer of $[\mathbf{A}]^{2-}$ with a transannular B–B bond is released. However, the associated activation energies should be high and corresponding structures have so far not been reported; the closest known relatives are 1,4-disila(Dewar-benzene)s: Kabe, Y.; Ohkubo, K.; Ishikawa, H.; Ando, W., 1,4-Disila(Dewar-benzene) and 1,4-Disilabenzene: Valence Isomerization of Bis(alkylsilacyclopropenyl)s. *J. Am. Chem. Soc.* **2000**, *122*, 3775.

(29) Rüchardt, C.; Gerst, M.; Ebenhoch, J., Uncatalyzed Transfer Hydrogenation and Transfer Hydrogenolysis: Two Novel Types of Hydrogen-Transfer Reactions. *Angew. Chem. Int. Ed.* **1997**, *36*, 1406.

(30) Braude, E. A.; Jackman, L. M.; Linstead, R. P., Hydrogen Transfer. Part II. The Dehydrogenation of 1:4-Dihydronaphthalene by Quinones. Kinetics and Mechanism. *J. Chem. Soc.* **1954**, 0, 3548.

(31) As a caveat we note that B–H bond-dissociation energies similar to those of frequently used H•-atom donors have been obtained for BH_3 adducts with neutral Lewis bases (especially *N*-heterocyclic carbenes). Yet, a competing H^--ion transfer scenario would require an energetically unfavorable charge separation as opposed to the case of $[\mathbf{A}\text{-}H_2]^{2-}$: (a) Ueng, S.-H.; Solovyev, A.; Yuan, X.; Geib, S. J.; Fensterbank, L.; Lacôte, E.; Malacria, M.; Newcomb, M.; Walton, J. C.; Curran, D. P., N-Heterocyclic Carbene Boryl Radicals: A New Class of Boron-Centered Radical. *J. Am. Chem. Soc.* **2009**, *131*, 11256; (b) Hioe, J.; Karton, A.; Martin, J. M.; Zipse, H., Borane-Lewis Base Complexes as Homolytic Hydrogen Atom Donors. *Chem. Eur. J.* **2010**, *16*, 6861; (c) Ueng, S-H.; Fensterbank, L.; Lacôte, E.; Malacria, M.; Curran, D. P., Radical Reductions of Alkyl Halides Bearing Electron Withdrawing Groups with N-Heterocyclic Carbene Boranes. *Org. Biomol. Chem.* **2011**, *9*, 3415; (d) Curran, D. P.; Solovyev, A.; Makhlouf Brahmi, M.; Fensterbank, L.; Malacria, M.; Lacôte, E., Synthesis and Reactions of N-Heterocyclic Carbene Boranes. *Angew. Chem. Int. Ed.* **2011**, *50*, 10294.

(32) von Grotthuss, E.; Nawa, F.; Bolte, M.; Lerner, H.-W.; Wagner, M., Chalcogen–Chalcogen-Bond Activation by an Ambiphilic, Doubly Reduced Organoborane. *Tetrahedron* **2019**, *75*, 26.

(33) Jedliński, Z. J.; Kurcok, P.; Nozirow, F., Synthesis of Polysilanes by Reductive Coupling of Dichlorosilanes Mediated with Alkali Metal/Crown Ether Supramolecular Complexes in a Homogeneous System. *Macromol. Rapid Commun.* **1997**, *18*, 483.

(34) Morris, D. F. C., The Lattice Energies of the Alkali Halides. *Acta Crystallographica* **1956**, *9*, 197.

(35) Deberitz, J.; Boche, G., *Industrielle Anorganische Chemie*. 4th ed.; Wiley-VCH: Weinheim, **2013**.

(36) For further examples of boron-centered nucleophiles, see: (a) Hübner, A.; Bolte, M.; Lerner, H.-W.; Wagner, M., Extensive Structural Rearrangements Upon Reduction of 9H-9-Borafluorene. *Angew. Chem. Int. Ed.* **2014**, *53*, 10408; (b) Hübner, A.; Kaese, T.; Diefenbach, M.; Endeward, B.; Bolte, M.; Lerner, H.-W.; Holthausen, M. C.; Wagner, M., A Preorganized Ditopic Borane as Highly Efficient One- or Two-Electron Trap. *J. Am. Chem. Soc.* **2015**, *137*, 3705; (c) Kaese, T.; Budy, H.; Bolte, M.; Lerner, H.-W.; Wagner, M., Deprotonation of a Seemingly Hydridic Diborane(6) to Build a B–B Bond. *Angew. Chem. Int. Ed.* **2017**, *56*, 7546; (d) Wu, D.; Li, Y.; Ganguly, R.; Kinjo, R., A Snapshot of Inorganic Janovsky Complex Analogues Featuring a Nucleophilic Boron Center. *Chem. Commun.* **2017**, *53*, 12734; (e) Kaese, T.; Trageser, T.; Budy, H.; Bolte, M.; Lerner, H.-W.; Wagner, M., A Redox-Active Diborane Platform Performs C(sp^3)-H Activation and Nucleophilic Substitution Reactions. *Chem. Sci.* **2018**, *9*, 3881; (f) Himmel, H.-J., Nucleophilic Neutral Diborane(4) Compounds with sp^3-sp^3-Hybridized Boron Atoms. *Eur. J. Inorg. Chem.* **2018**, 2139; g) Zhao, Q.; Dewhurst, R. D.; Braunschweig, H.; Chen, X., A New Perspective on Borane Chemistry: The Nucleophilicity of the B–H Bonding Pair Electrons. *Angew. Chem. Int. Ed.* **2019**, *58*, 3268.

(37) CO_2 reduction by $NaBH_4$ has already been reported: Knopf, I.; Cummins, C. C., Revisiting CO_2 Reduction with $NaBH_4$ under Aprotic Conditions: Synthesis and Characterization of Sodium Triformatoborohydride. *Organometallics* **2015**, *34*, 1601.

(38) Gilbert, A.; Cooper, G.; Shade, R., Alkylchlorosilanes. Reduction of Alkylchlorosilenes by Sodium Hydride and Hydrogen-Chlorine Interchange in Chlorosilanes. *Ind. Eng. Chem.* **1959**, *51*, 665.

(39) Pachaly, B.; Achenbach, F.; Herzig, C.; Mautner, K., *Silicone*; Wiley-VCH: Weinheim, **2005**.

(40) Sommer, L. H.; Golino, C. M.; Roark, D. N.; Bush, R. D., Reduction of Silicon Halides and Alkoxides with Diisobutylaluminum Hydride. Stereochemistry-Rate Law Correlations for the S_Ni–Si and S_N2–Si Mechanisms. *J. Organomet. Chem.* **1973**, *49*, C3.

(41) (a) Houghton, A. Y.; Hurmalainen, J.; Mansikkamaki, A.; Piers, W. E.; Tuononen, H. M., Direct Observation of a Borane-Silane Complex Involved in Frustrated Lewis-Pair-Mediated Hydrosilylations. *Nature Chem.* **2014**, *6*, 983; (b) Brook, M. A., New Control over Silicone Synthesis Using SiH Chemistry: The Piers-Rubinsztajn Reaction. *Chem. Eur. J.* **2018**, *24*, 8458.

(42) (a) Budanow, A.; Sinke, T.; Tillmann, J.; Bolte, M.; Wagner, M.; Lerner, H.-W., Two-Coordinate Gallium Ion $[t\text{Bu}_3\text{Si–Ga–Si}t\text{Bu}_3]^+$ and the Halonium Ions $[t\text{Bu}_3\text{Si–X–Si}t\text{Bu}_3]^+$ (X = Br, I): Sources of the Supersilyl Cation $[t\text{Bu}_3\text{Si}]^+$. *Organometallics* **2012**, *31*, 7298; (b) Budanow, A.; Bolte, M.; Wagner, M.; Lerner, H.-W., The Ion-Like Supersilylium Compound $t\text{Bu}_3\text{Si–F–Al}[\text{OC}(\text{CF}_3)_3]_3$. *Eur. J. Inorg. Chem.* **2015**, 2524.

(43) (a) Reus, C.; Weidlich, S.; Bolte, M.; Lerner, H.-W.; Wagner, M., C-Functionalized, Air- and Water-Stable 9,10-Dihydro-9,10-diboraanthracenes: Efficient Blue to Red Emitting Luminophores. *J. Am. Chem. Soc.* **2013**, *135*, 12892; (b) John, A.; Bolte, M.; Lerner, H.-W.; Wagner, M., A Vicinal Electrophilic Diborylation Reaction Furnishes Doubly Boron-Doped Polycyclic Aromatic Hydrocarbons. *Angew. Chem. Int. Ed.* **2017**, *56*, 5588; (c) Kirschner, S.; Mewes, J. M.; Bolte, M.; Lerner, H.-W.; Dreuw, A.; Wagner, M., How Boron Doping Shapes the Optoelectronic Properties of Canonical and Phenylene-Containing Oligoacenes: A Combined Experimental and Theoretical Investigation. *Chem. Eur. J.* **2017**, *23*, 5104; (d) Brend'amour, S.; Gilmer, J.; Bolte, M.; Lerner, H.-W.; Wagner, M., C-Halogenated 9,10-Diboraanthracenes: How the Halogen Load and Distribution Influences Key Optoelectronic Properties. *Chem. Eur. J.* **2018**, *24*, 16910; (e) John, A.; Kirschner, S.; Fengel, M. K.; Bolte, M.; Lerner, H.-W.; Wagner, M., Simultaneous Expansion of 9,10 Boron-Doped Anthracene in Longitudinal and Lateral Directions. *Dalton Trans.* **2019**, *48*, 1871.

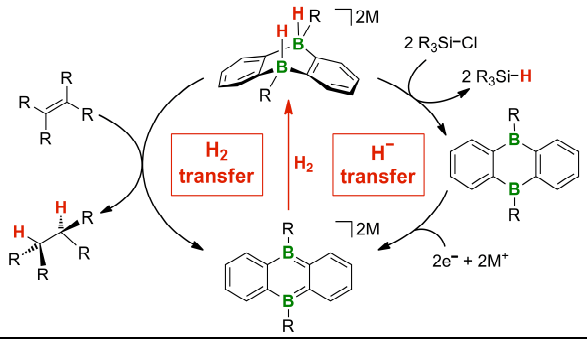
H
R
2M
H
B
B
R
2 R3Si–Cl
2 R3Si–H
R
R
R
R
B
B
R
H2 transfer
H2
H– transfer
H
R
H
R
R
R
2M
R
B
B
R
2e– + 2M+

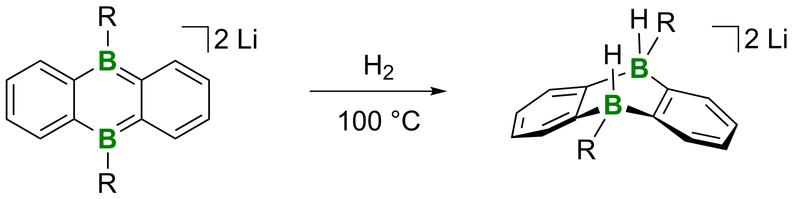

Li_2[**A**] Li_2[**A**-H_2]

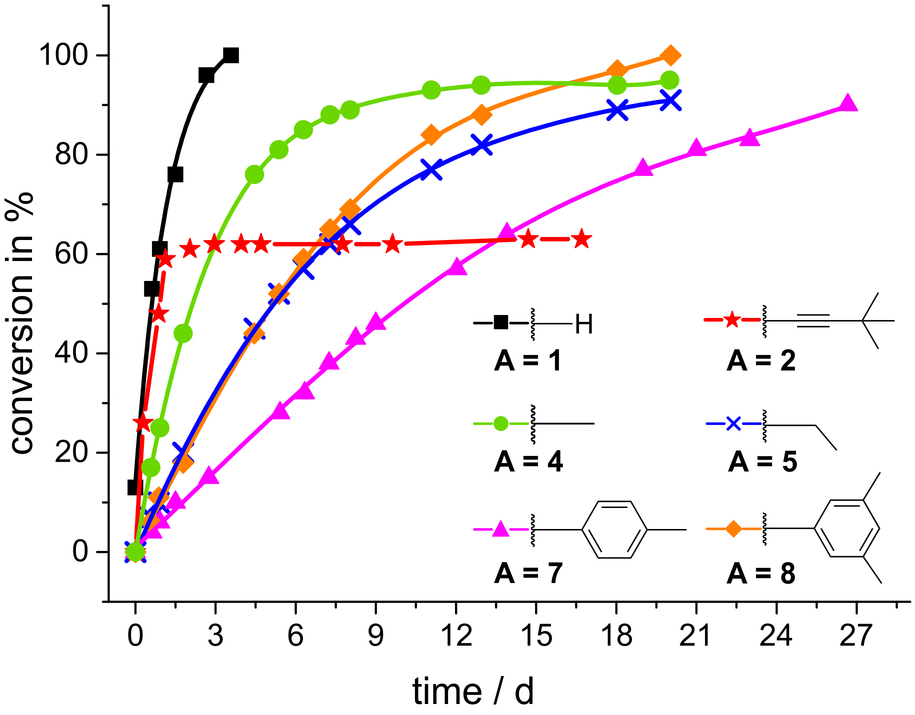

Figure1

84x86mm (300 x 300 DPI)

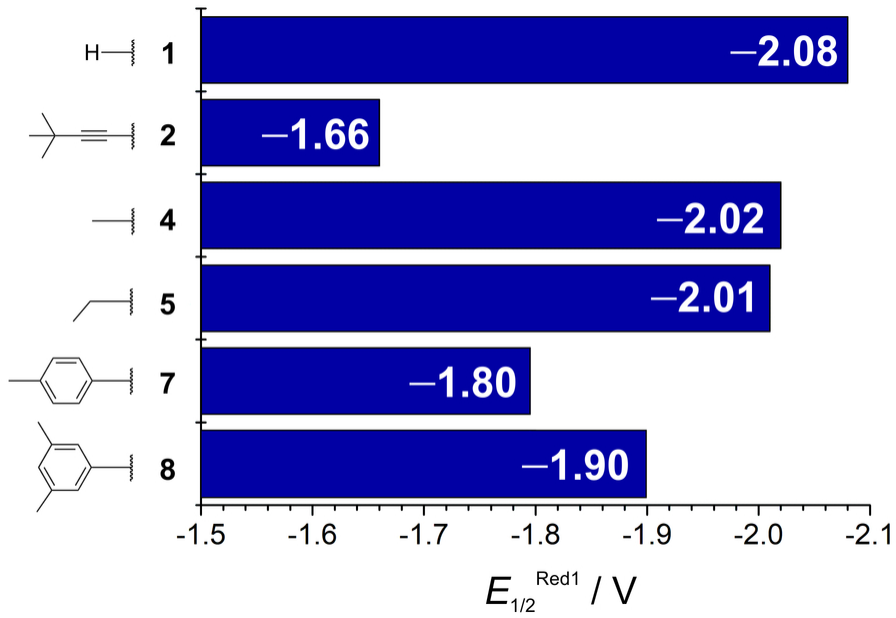

Figure2

84x54mm (300 x 300 DPI)

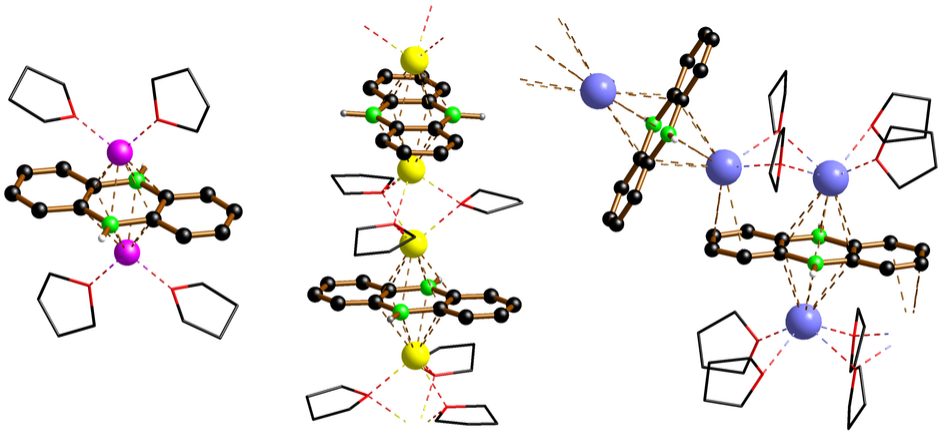

$[Li(thf)_2]_2[\mathbf{1}]$ $\{[Na_2(thf)_3][\mathbf{1}]\}_n$ $\{[K_2(thf)_4][\mathbf{1}]\}_n$

84x44mm (300 x 300 DPI)

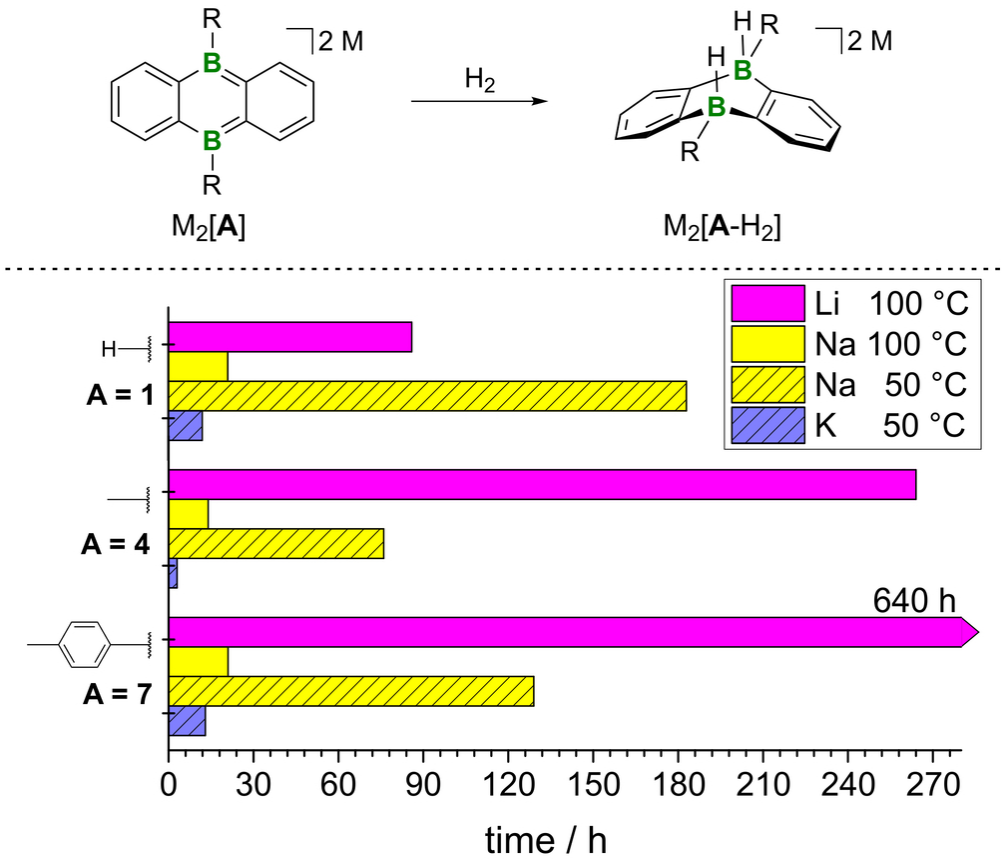

84x74mm (300 x 300 DPI)

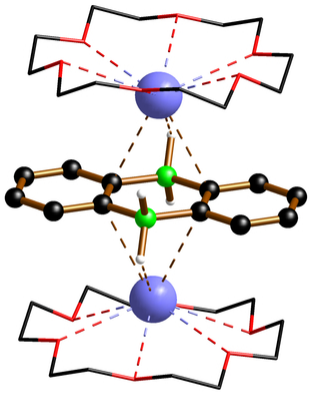

[K(18-c-6)]$_2$[**1**-H$_2$]

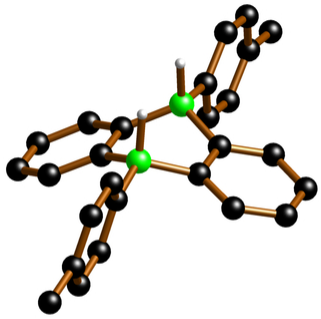

[**7**-H$_2$]$^{2-}$

84x44mm (300 x 300 DPI)

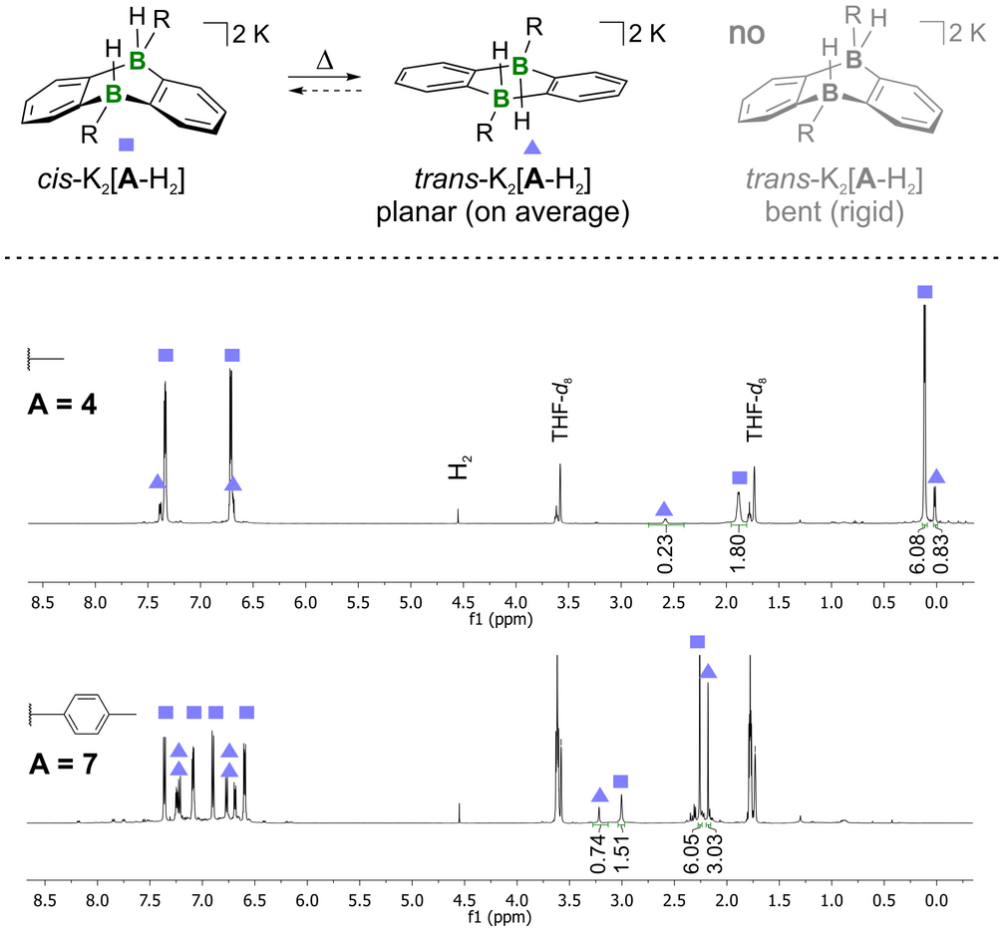

84x80mm (300 x 300 DPI)

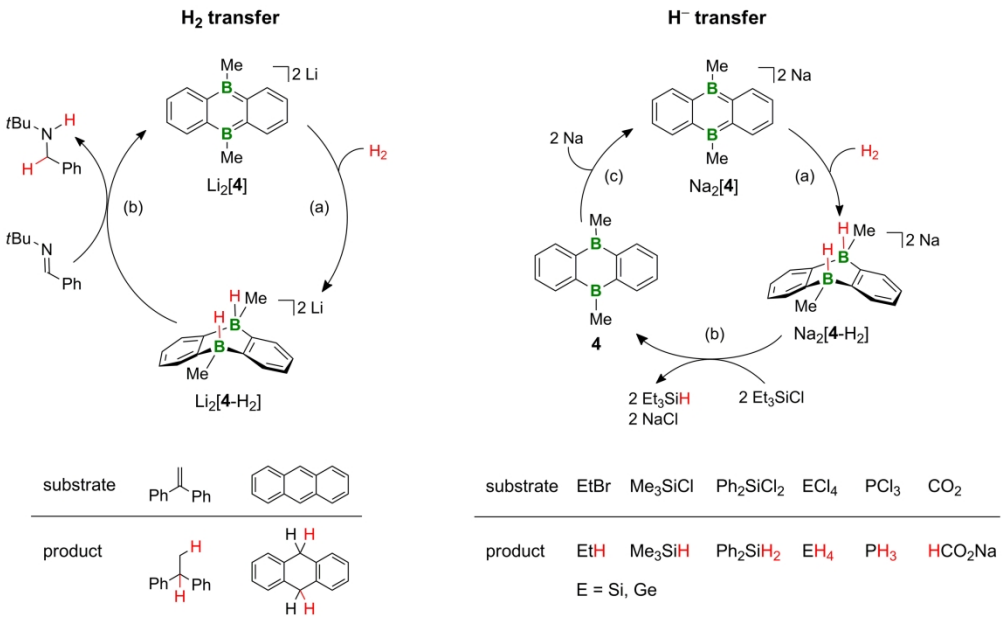

259x160mm (300 x 300 DPI)

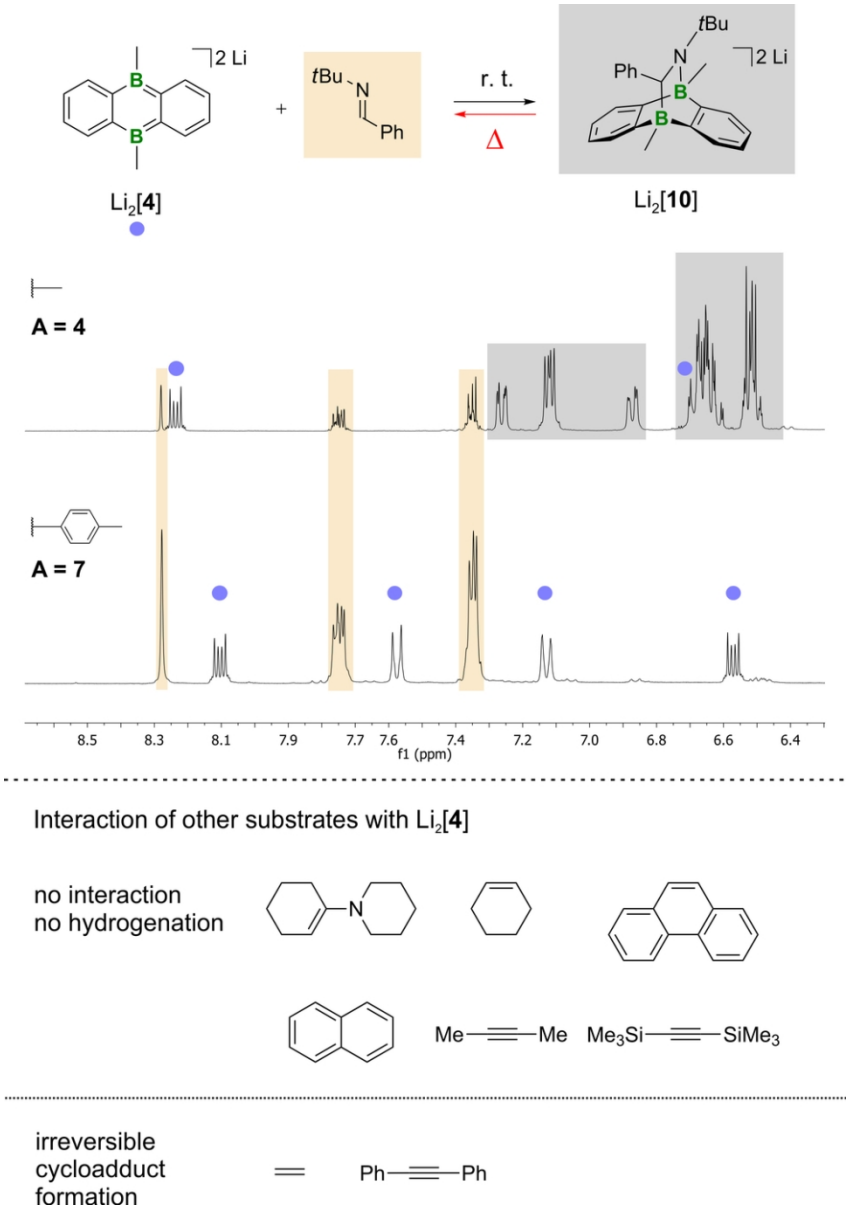

Figure8

84x120mm (300 x 300 DPI)

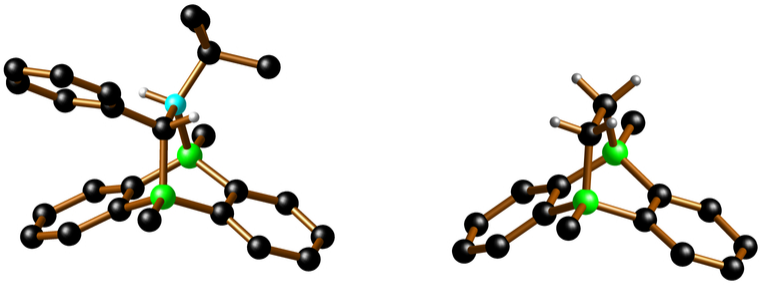

H[**10**]$^{-}$ [**11**]$^{2-}$

84x33mm (300 x 300 DPI)

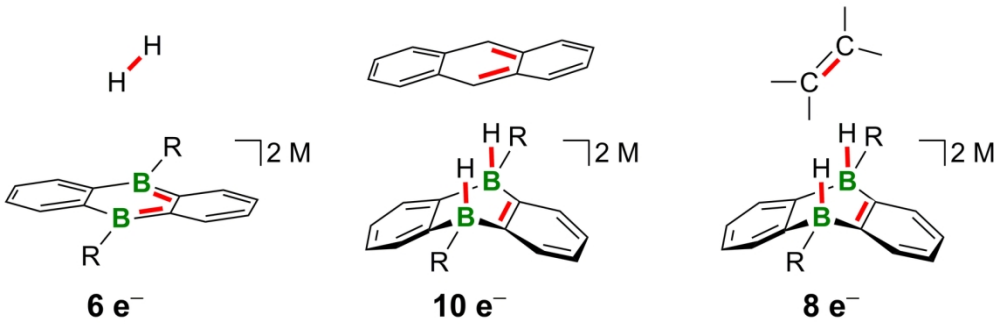

156x51mm (300 x 300 DPI)

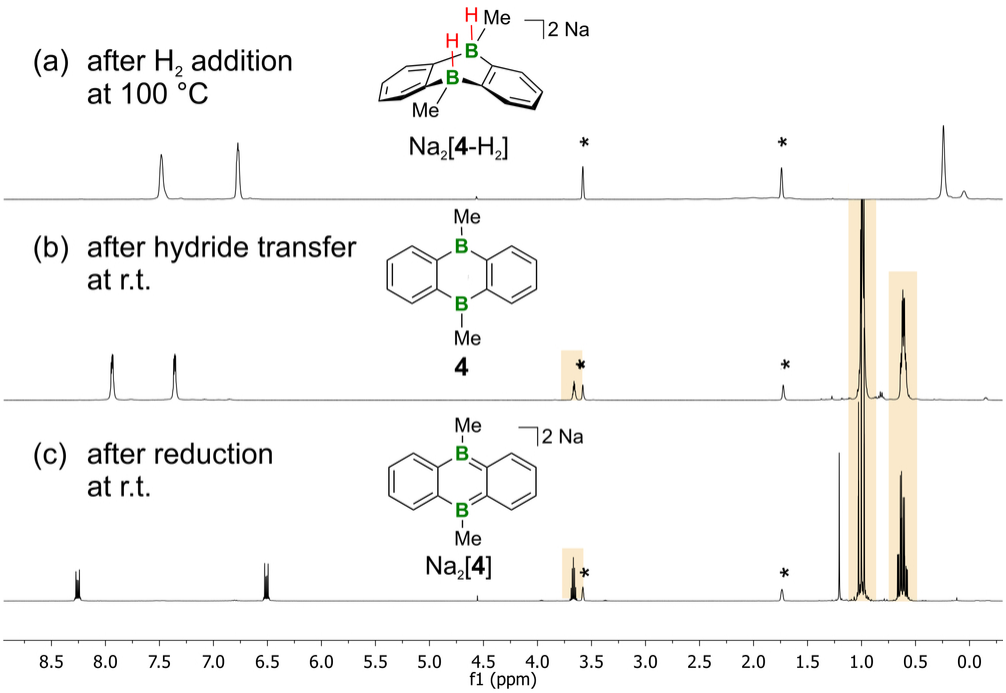

84x60mm (300 x 300 DPI)

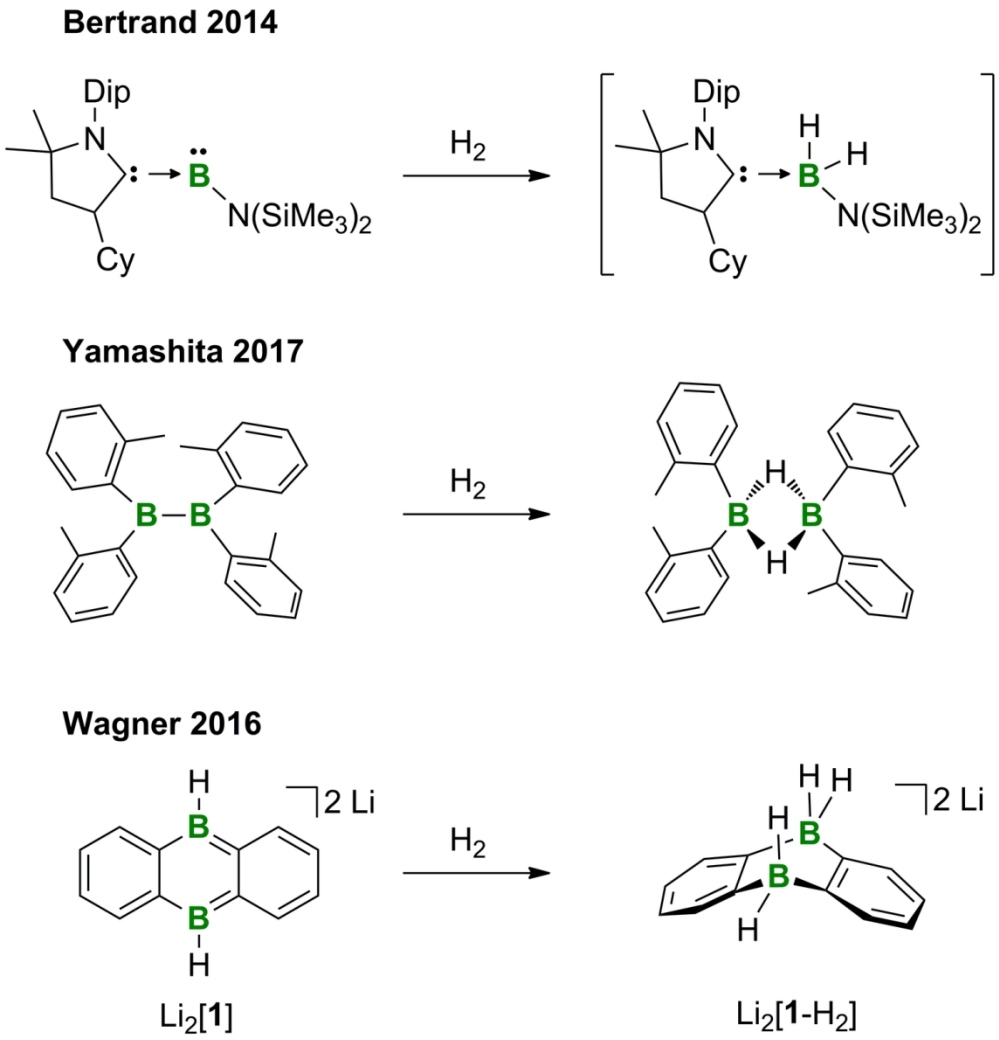

130x136mm (300 x 300 DPI)

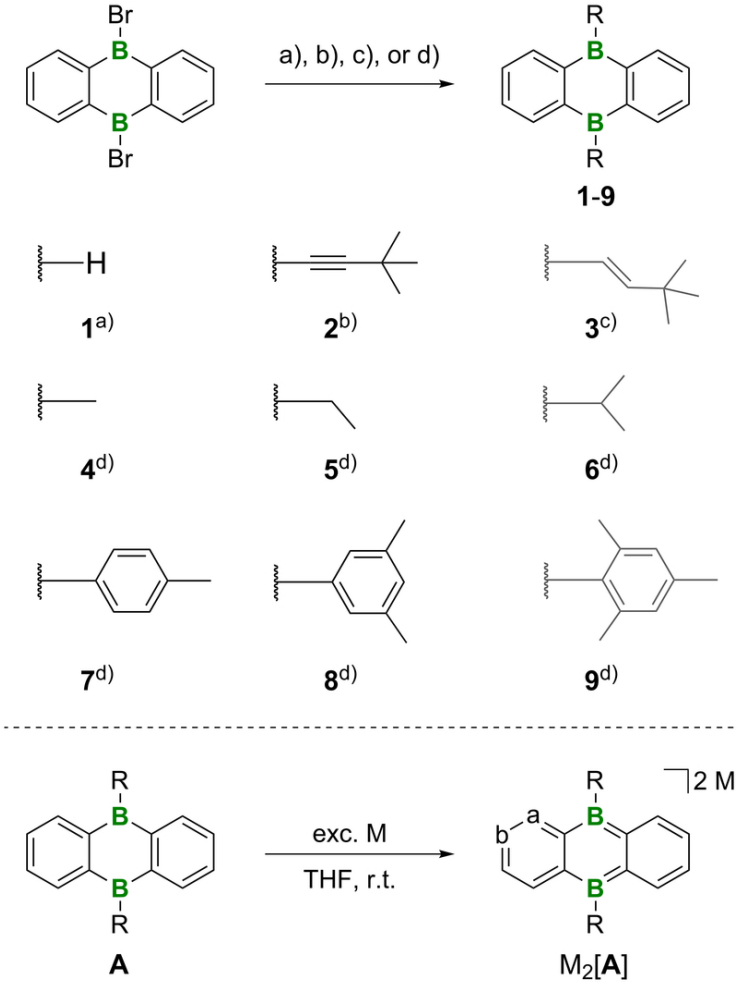

M_2[**A**]	**A = 1**	**2**	**3**	**4**	**5**	**7**	**8**	**9**
M = Li	✓	✓	✓	✓	✓	✓	✓	✓
Na	✓	✓	–	✓	–	✓	–	–
K	✓	×	–	✓	✓	✓	✓	–

84x109mm (300 x 300 DPI)

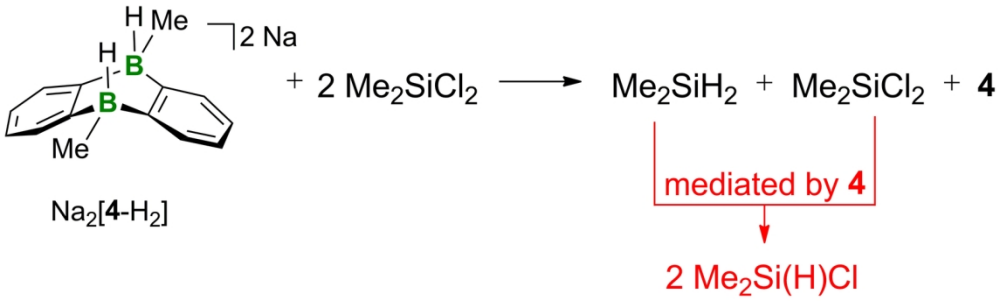

152x46mm (300 x 300 DPI)

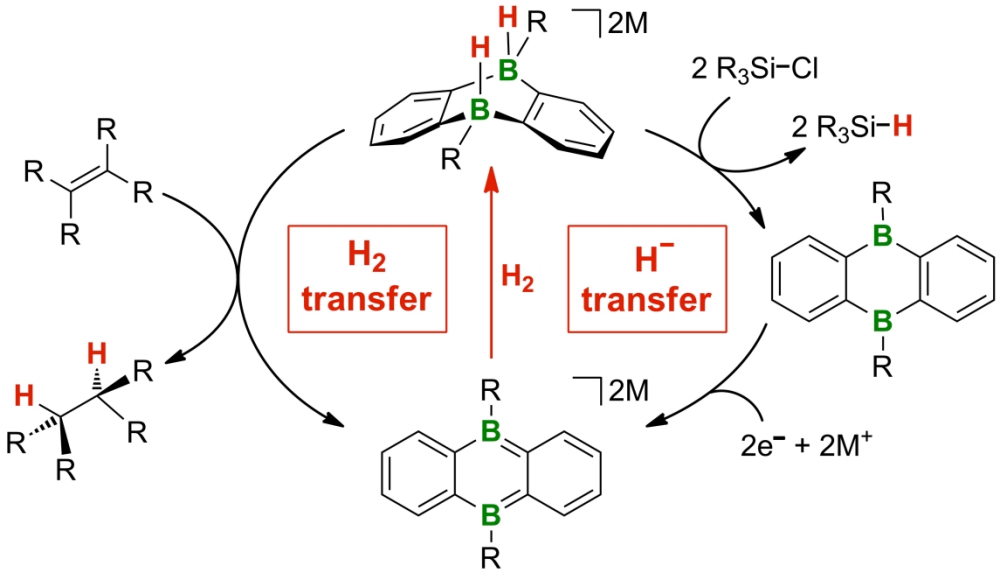

Table of Content

142x81mm (600 x 600 DPI)